

Mesoscale airflow structure over the northern Croatian coast during MAP IOP 15 – a major bora event

*Zvezdana Bencetić Klaić^a, Danijel Belušić^a, Vanda Grubišić^b,
Lada Gabela^a and Ladislav Čoso^a*

^a Andrija Mohorovičić Geophysical Institute, Faculty of Science, University of Zagreb, Zagreb, Croatia

^b Division of Atmospheric Sciences, Desert Research Institute, Reno, NV, USA

Received 4 December 2002, in final form 2 December 2003

We have investigated a strong Bora event over the Northern Adriatic, which occurred on 7 November 1999 during MAP IOP 15. The wind field, potential temperature, vertical component of relative vorticity, and turbulent kinetic energy in the lower troposphere were simulated by a nonhydrostatic mesoscale model (MEMO), which was run at a very fine horizontal resolution with the grid spacing of 1 km. Our model simulation accurately reproduced the timing of the Bora event, and the modeled fields exhibited a good agreement with routinely measured winds along the Croatian coast as well as a large degree of consistence with the MAP measurements offshore. The model results also provided a detailed view of the hydraulic airflow structure and thermodynamic conditions during the Bora event. Our simulation results confirm the existence of topographically induced vorticity filaments originating in the turbulent regions near the coastal mountains, where these turbulent zones are collocated with the hydraulic jump-like flow features. All of the above processes have the highest intensity in the region of Senj.

Keywords: Bora, hydraulic flow, northern Adriatic

1. Introduction

The Mesoscale Alpine Programme (MAP) is an international research program aimed at improving both the theoretical knowledge and numerical prediction of weather and climate over complex topography. An extensive field experiment, the Special Observation Period (SOP) of MAP, took place in the Alpine region, including the Northern Adriatic, from 7 September to 15 November 1999. The primary scientific objectives of this particular MAP phase were focused on orographically influenced precipitation events (including frontal precipitation and deep convection) and consequent flooding episodes, Foehn-related phenomena, three-dimensional gravity wave breaking and associated wave drag, high altitude potential vorticity (PV) anomalies

(PV streamers) and low-altitude orographically-generated PV anomalies (PV banners). During one of the MAP Intensive Observation Periods (IOP), namely MAP IOP 15, a strong Bora event occurred over the Northern Adriatic, and was documented as part of the MAP PV banner project on November 7, 1999. This is the case on which we focus in this study.

Among others, the Bora wind at the Adriatic coast was investigated by Makjanić (1970, 1976, 1978), who focused on the climatology and diurnal variation of the wind speed. The climatological analysis was also performed by Orlić et al. (1994) and Heimann (2001). Orlić et al. studied the Bora-driven currents and sea-level changes in the Adriatic. For this purpose they calculated the Bora wind stress along the Croatian coast based on 10-year data. They obtained four peaks, which were associated with topography, and whose positions roughly correspond to Pula, Senj, Split and Makarska, respectively, with the value of stress at Senj being the largest. Based on the climatological synoptic scale data over Europe, Heimann suggested four typical mean geopotential height patterns associated with the Bora events.

Jurčec (1981) was the first to emphasize the importance of interaction of processes on various scales of motion for the Bora characteristics. She showed how large-scale anomalies may change mesoscale characteristics of the Bora environment, leading to a relatively warm Bora. Vučetić (1984) pointed out the existence of large wind shear in the upstream region during the Bora event, and the neutral stability of the Bora layer. When the Bora is very strong, the Bora layer is covered on top with a stable layer. Koračin (1984) investigated parameters, such as the Brunt-Väisälä frequency and Froude number, and, showed that with a well-developed Bora layer, differences between flow parameters on the windward and leeward side become smaller compared to the same at the beginning and the end of the Bora event.

Smith (1987) related the dynamics of Bora to the hydraulic theory. The same approach was followed by Grubišić (1989) and Bajić (1991) for Bora cases on the Northern Adriatic characterized with the strong upstream flow. Smith also pointed out Bora's similarity to the Boulder windstorm. He emphasized several common features of the Bora events: i) an upstream descent and acceleration beginning where the mountains rise; ii) an approximate coincidence between the depth of the uppermost descending streamline and a wind reversal level (when such a reversal exists); iii) a decoupling of the flow aloft associated with a splitting of the inversion and the formation of a thick mixed layer downstream; iv) a narrow region of intense turbulence, and v) an ascending jet just downstream of the plunging Bora. Similarly, Qian and Giraud (2000), based on the simulation of one case of a typical Bora with a stationary cyclone over the southern Adriatic Sea, point out prevalent Bora features, as the upstream acceleration, the strong descent within the Bora layer and the turbulent zone just downstream of the mountains.

Ivančan-Picek and Tutiš (1996) identified Bora cases in which hydraulic theory could not be applied, addressing a generally less investigated Bora on

the Southern Adriatic. Their results confirmed the multiscale nature of the Bora-related airflow. Furthermore, they unravel an essential role of the downstream effects on the Bora genesis due to the isallobaric component of the ageostrophic motion. Therefore, they conclude that the Southern Adriatic Bora mechanism could not be explained by the 2-D hydraulic theory with simple upstream conditions, as it is mainly the case for the Bora on the Northern Adriatic.

A number of investigators have performed numerical experiments in order to investigate impacts of different conditions on the Bora development. Petkovšek (1990) suggested two main factors affecting the wind speed. One is the stability of the 'environmental' warm air found above the cold Bora air, and the other, more important, is the temperature difference between the two air masses. The same author performed additional numerical experiments with the frontal Bora model (Petkovšek, 1991), in which the upper boundary of the Bora is treated as a dynamically balanced frontal surface. His results indicate the following: 1) a higher ridge and greater inclination of the slope cause a higher Bora speed; 2) absolute temperature (*i.e.* season) has only a small influence on the Bora speed; and 3) the shape of the lee side slope affects the Bora only moderately.

Enger and Grisogono (1998) studied the effects of difference between the sea-surface and land temperature (mesoscale forcing) as well as the geostrophic wind direction (synoptic forcing) on the idealized Bora cases. They concluded that an offshore propagating hydraulic jump, associated with the Bora front, is induced by a lee-side low pressure, where the latter is due either to the mesoscale or synoptic forcing. Thus, both the synoptic situation and the state of marine atmospheric boundary layer are crucial for the Bora development. Lazić and Tošić (1998) employed different heights and shapes of the mountains in their Bora simulations. The Bora developed only in the presence of the control mountains in the region, which have the average height of about 1000 m. For decreased mountains heights, a corresponding decrease of air accumulation in front of the mountain barrier occurred. When the heights were increased, the blocking effect of the mountains deformed the Bora flow.

The objectives of this study are:

1. To validate performance of the mesoscale nonhydrostatic model MEMO (Moussiopoulos, 1994, 1995; Kunz and Moussiopoulos, 1995) over the Northern Adriatic for the case of a strong Bora event,
2. To investigate the mesoscale thermodynamic and airflow conditions, namely wind field, potential temperature (θ), vertical component of relative vorticity ($\xi = \frac{\partial v}{\partial x} - \frac{\partial u}{\partial y}$) and turbulent kinetic energy (*TKE*) fields, within the

lower troposphere during this particular Bora event using the model solutions and the MAP IOP data, and

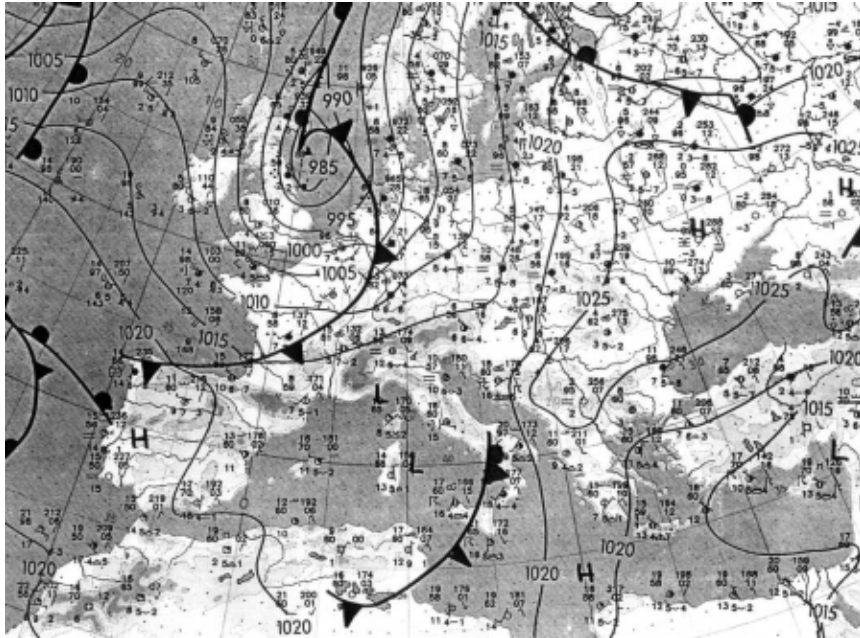
3. To examine in more detail atmospheric conditions in the region of Senj since frequent and severe Bora events occur there often (Makjanić, 1976, 1978; Bajić, 1987).

An in depth analysis of the MAP IOP 15 Bora case is presented in Grubišić (2004), where the dynamics and structure of the lee-side and cross-mountain flow past the coastal mountains were investigated using the aircraft and other *in situ* and remotely sensed data from the MAP IOP mission over the Adriatic together with the high-resolution mesoscale simulations with the Naval Research Laboratory (NRL) Coupled Ocean-Atmosphere Modeling System (COAMPS), carried out at the horizontal resolution of 3 km. That study focused on the structure and origin of the orographically-generated PV banners over the Adriatic, which were shown to be accurately simulated by the COAMPS model at that horizontal resolution, and to originate in dissipative regions in the proximity of the coastal terrain. The same MAP IOP 15 Bora episode was studied also by Tudor and Ivatek-Šahdan (2002), who focused solely on the ability of the ALADIN model to forecast severe Bora winds. In this study we employ a finer model horizontal resolution (1 km) than previously used in the studies of this Bora case. The model results at this high resolution enabled us to gain a very detailed insight into the structure of the Bora flow and the associated conditions in the lower troposphere.

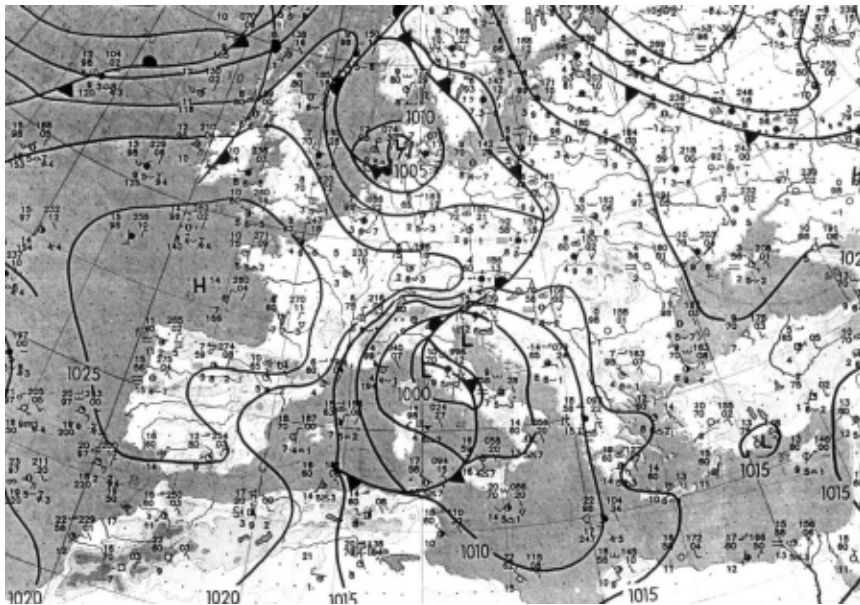
2. Synoptic Conditions

The analysis of synoptic conditions during this Bora event presented here is based on the surface and upper-level diagnostic charts over Europe. These synoptic products were available at every six (00, 06, 12 and 18 UTC), and twelve hours, respectively. Here, both the surface (Figure 1) and the upper-level charts (Figure 2) are shown for 00 and 12 UTC times only. By 06 UTC on 6 November 1999, a deep surface cyclone had moved eastward over the North Sea. A cold front, extending from Denmark to southern France, was moving toward the Alps. Upper-level charts show a cutoff from a southward oriented trough, which at 12 UTC was found over the North Sea. Associated strong northwesterly cold-air advection toward the Mediterranean led to the lee cyclogenesis over the Gulf of Genoa south of the Alps.

Subsequent to 18 UTC on 6 November the center of the surface Genoa cyclone was found over the central Italy and the Tyrrhenian Sea. Simultaneously, two high-pressure centers were present over the European continent. One was centered over the northwestern France and the eastern Atlantic, reaching to Germany and the Czech Republic and establishing a relatively high, north-south synoptic pressure gradient. This anticyclone together with the Genoa cyclone favored the development of the Bora wind over

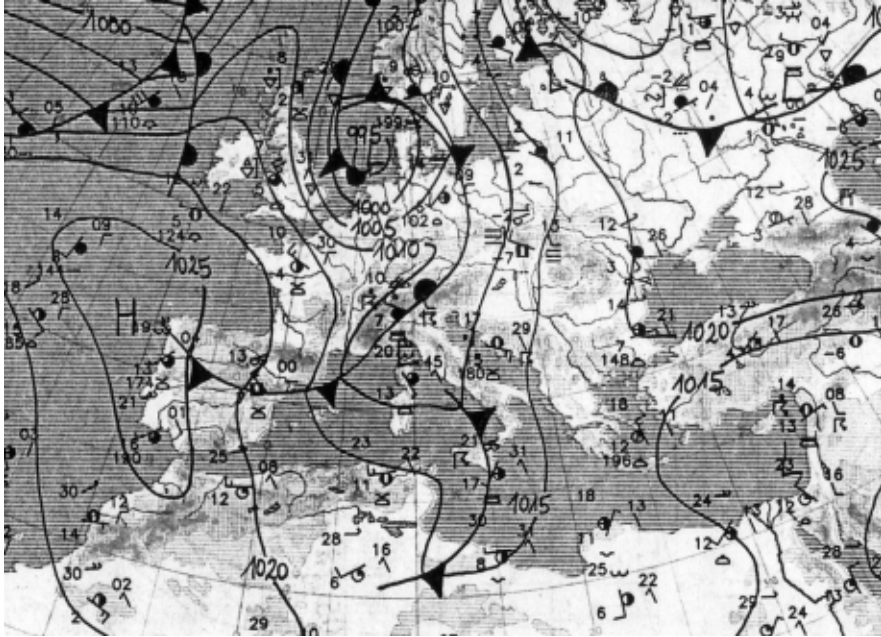


6 November 1999, 00 UTC

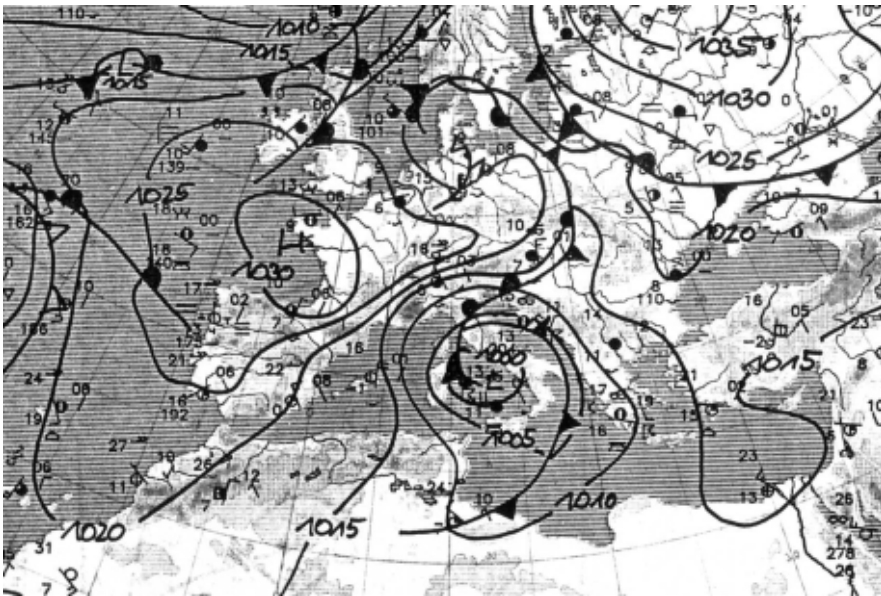


6 November 1999, 12 UTC

Figure 1. Surface diagnostic charts over Europe for 6–7 November 1999.



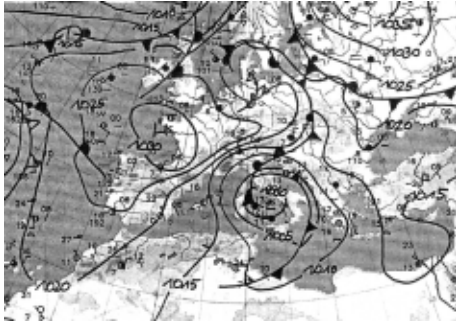
7 November 1999, 00 UTC



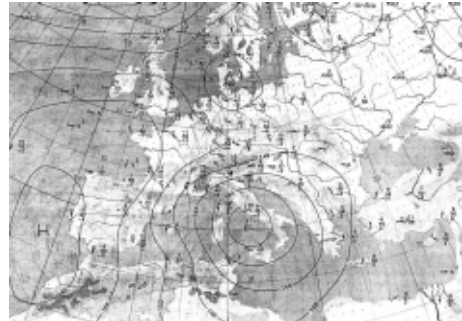
7 November 1999, 12 UTC

Figure 1. cont.

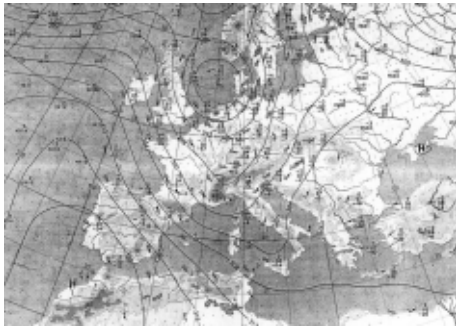
the Northern Adriatic, which started in late hours of 6 November. The other anticyclone was positioned over the northwestern Russia.



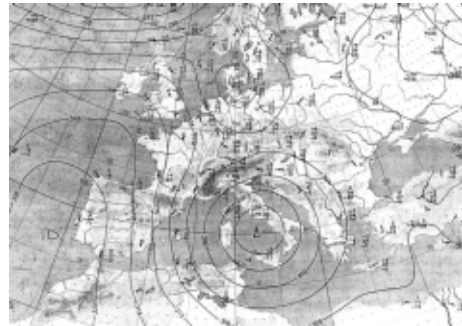
6 November 1999, 12 UTC, 850 hPa



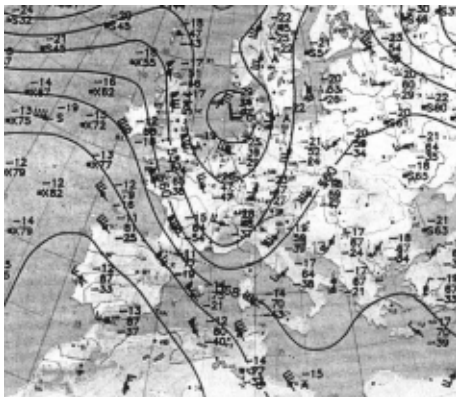
7 November 1999, 12 UTC, 850 hPa



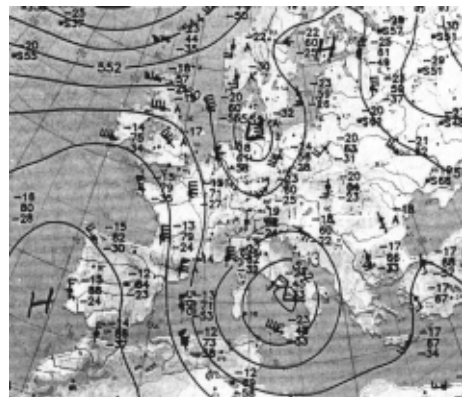
6 November 1999, 12 UTC, 700 hPa



7 November 1999, 12 UTC, 700 hPa



6 November 1999, 12 UTC, 500 hPa



7 November 1999, 12 UTC, 500 hPa

Figure 2. Upper level 850, 700 and 500 hPa diagnostic charts over Europe (top, center and bottom, respectively), for 6 and 7 November 1999 at 12 UTC.

During 7 November (see Figures 1 and 2), the center of the surface Genoa cyclone moved slowly towards the southeast, and was accompanied with the upper-level cyclonic vortex. At the same time, the anticyclone over western Europe became elongated extending towards the east. Consequently, the southward pressure gradient increased and the Bora over the Northern Adriatic continued to strengthen. The above synoptic situation, which is characterized with a cut-off low over the Adriatic, is very similar to one of the four typical synoptic patterns associated with the Bora wind at the Croatian coast in winter months (Heimann, 2001).

3. Observational Data

During this Bora event, standard surface wind measurements were available at four coastal sites (Pazin, Pula, Rijeka, and Senj). Additionally, the wind speed data only were available at the Krk Bridge location. The positions of these measuring sites are shown in Figure 3. In addition to the routine surface data, in this study we have used the aircraft data from the MAP IOP 15 for 7 November 1999. The MAP IOP 15 data used here were obtained by the National Center for Atmospheric Research (NCAR) aircraft Electra (Grubišić, 2004) between 14:30 UTC and 15:42 UTC flying along tracks parallel to the Croatian coast at approximately 300 m and 600 m ASL.

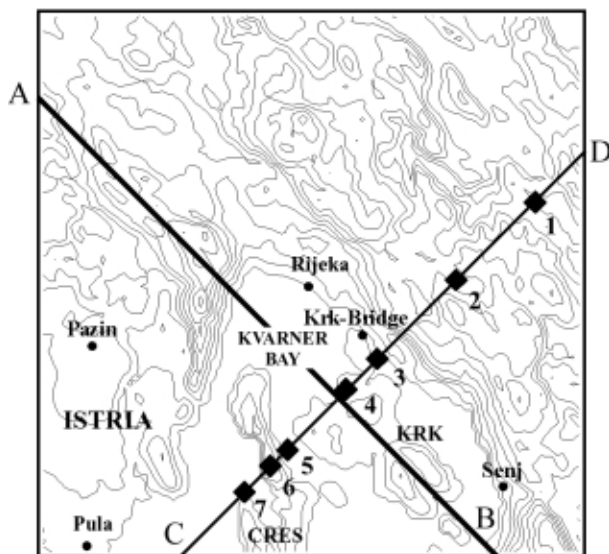


Figure 3. The 100×100 km² grid domain. Topography contours are shown every 150 m. The domain center is over Rijeka (45.33 °N, 14.45 °E, 120 m ASL). The solid circles indicated positions of the available routine measuring sites. Line AB is parallel Electra track, and it is the base of the vertical cross-section shown in Fig. 8. Line CD, parallel to the direction of the Bora flow, is the base of the vertical cross-sections displayed in Figs. 14–16. Points 1–7 along the line CD are discussed in section 4.3.

4. Numerical Simulation

We employed an Eulerian nonhydrostatic prognostic mesoscale model for an unsaturated atmospheric boundary layer (MEMO, version 6.0). Model description and its performance have been documented previously (Moussiopoulos, 1994, 1995; Kunz and Moussiopoulos, 1995; Moussiopoulos et al., 1997a, 1997b; Klaić et al., 2002, Klaić and Nitis, 2001–2002, Klaić et al., 2003). The model vertical coordinate is terrain following. Boundary conditions for the wind velocity components, potential temperature and pressure are specified as in Moussiopoulos (1994). At open boundaries, wave reflection and deformation is minimized by the use of modified 'radiation conditions' (Carpenter, 1982). For the nonhydrostatic part of the mesoscale pressure perturbation, homogenous Neumann boundary conditions are used at the lateral boundaries, where the wind velocity component perpendicular to the boundary remains unaffected by the pressure change. At the upper boundary, Neumann boundary conditions are imposed for the horizontal velocity components and the potential temperature, whereas the radiative condition is applied for the hydrostatic part of the mesoscale pressure perturbation. For the nonhydrostatic part of the mesoscale pressure perturbation, a homogenous staggered Dirichlet conditions and the 'no-flow-through' conditions are imposed for the upper and lower boundary, respectively. All other conditions at the lower boundary follow from the Monin-Obuhkov similarity theory.

The simulation was performed for the period from 5 to 7 November 1999, in which the first day was taken for the pre-run purposes. The model was driven with the Zagreb-Maksimir (45.82 °N, 16.03 °E, 128 m ASL) radiosonde data, which were available at 00 and 12 UTC on November 5, at 12 and 15 UTC on November 6, and at 00, 12, 15 and 24 UTC on November 7. This simulation was performed at the horizontal resolution of 1 km and the time increment of 5 seconds. The center of the 100 × 100 km² domain (Fig. 3) was placed over the Rijeka measuring site (45.33 °N, 14.45 °E, 120 ASL), which is about 130 km southwest of Zagreb. The model top was set at 6000 m above the surface. In the vertical, 25 layers were selected with a finer resolution at lower altitudes. Layer depths gradually increased from 20 m at the bottom to about 900 m at the top of the modeling domain.

Seven landuse types were assumed. Corresponding short-wave albedos, evaporation parameters, volumetric heat capacities, thermal soil conductivities and roughness lengths for all landuse types except the forest and urban were taken as in the study of Klaić et al. (2002). Employed roughness lengths for the forested and urban surfaces were 0.4 m and 0.9 m, respectively.

5. Results and Discussion

Figure 4 illustrates the modeled versus measured surface winds for the available measuring sites, which are indicated in Figure 3. Except for the Pula airport and the Krk Bridge site, the measured values correspond to the hourly means, whereas the modeled values are the instantaneous values at a particular round hour. For Pula, the measured values are given by the mean, determined from the 10-minute measurement intervals starting 10 minutes prior to the round hour.

It is apparent that the wind speeds are satisfactorily predicted for all five sites for times prior to the onset of Bora, which started in the evening hours of November 6. However, during the Bora, the modeled speeds for Senj and Rijeka are substantially higher than measured (sometimes by more than 15 m s^{-1}), with somewhat lower model overestimation for the Krk Bridge and Pazin. On the other hand, predicted wind speeds for Pula are lower than those measured.

To some extent the model overestimation at four out of five selected sites could be attributed to the smoothed topography employed in our simulations. However, this particular Bora event is considered to be one of the strongest Boras on record in recent decades (Grubišić, 2000). For such a strong Bora the expectation is that the real wind speeds in Senj, which is located below the Vratnik Pass and thus exposed to frequent and severe Bora events due to the channeling effects of the pass, were higher than those shown in the hourly averages in Figure 4. Our expectations were confirmed in the discussion with the staff of the Meteorological and Hydrological Service of Croatia (Vučetić, 2002), who indicated that both Senj and Rijeka measured maximal values are questionable due to the lee side positions of the two measuring sites.

Unlike wind speeds, wind directions are well predicted at all available measuring sites. The agreement is particularly good during the Bora duration for Senj, Rijeka and Pula. For Pazin discrepancies are slightly higher but they do not exceed 90° . Consequently, the timing of the Bora event is also well predicted.

Figure 5 shows modeled surface winds for 6 and 7 November. Throughout November 6 winds were weak, and until 18 UTC they were predominantly southerly, which is in agreement with the synoptic situation (Figs. 1 and 2). At 18 UTC a pronounced northerly flow developed, though the wind speeds were still weak. As seen from the surface synoptic chart (not shown here), the Genoa cyclone, which supports such airflow, has by then become well established and centered over the central Italy and the Tyrrhenian Sea. The ridge of the western anticyclone, which is the second factor contributing to the north-south synoptic pressure gradient has also by then stretched toward the east, being located to the north of the Genoa cyclone. Starting at 00 UTC on November 7 the northeasterly wind is strongest over the Kvarner

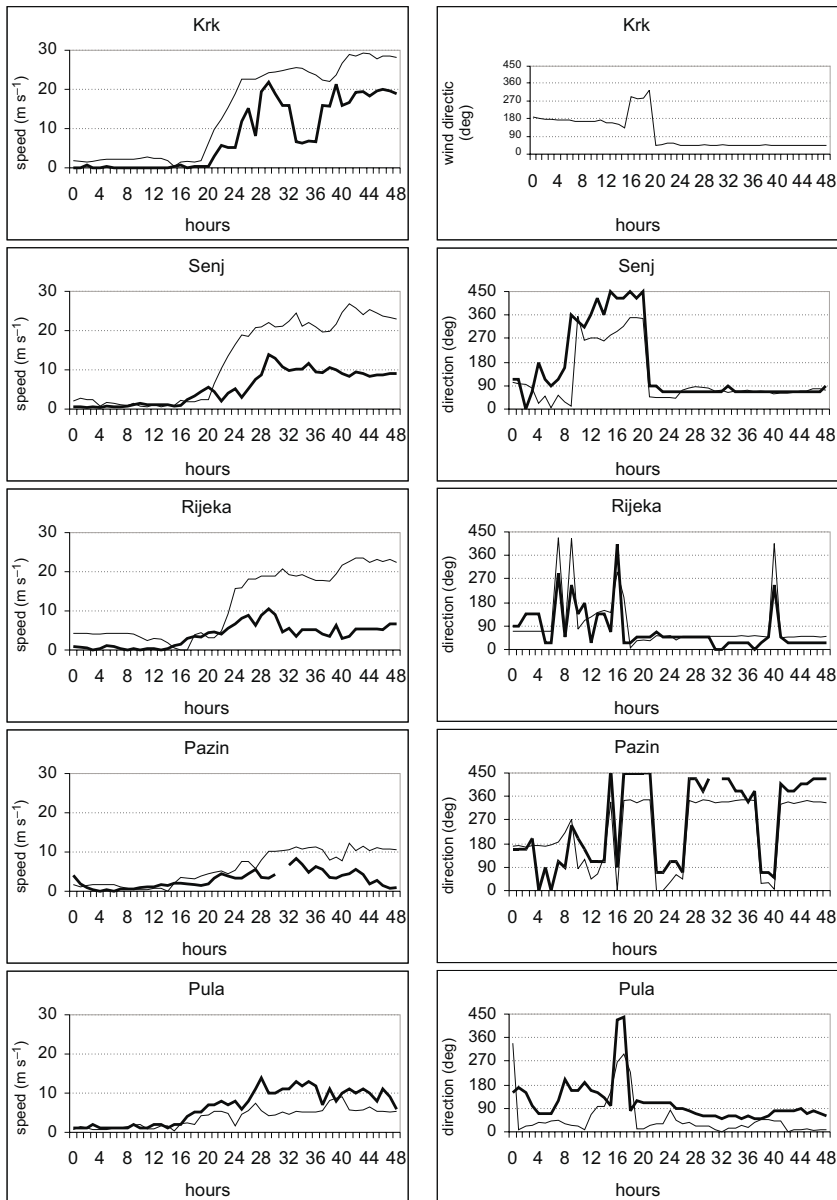


Figure 4. Modeled (thin line) versus measured (heavy line) surface winds (10 m above the ground) for 6 and 7 November 1999. Positions of the measuring sites are indicated in Figure 3. Note that some of the wind directions in the range from 0 to 90 degrees were shifted by 360 degrees in order to facilitate an easier visual comparison of the measured with the model-predicted values. This was done only in cases in which an otherwise small difference in the observed and modeled wind directions (e.g. 10 degrees and 340 degrees) would produce an unrealistically large error due to the circular nature of the wind rose.

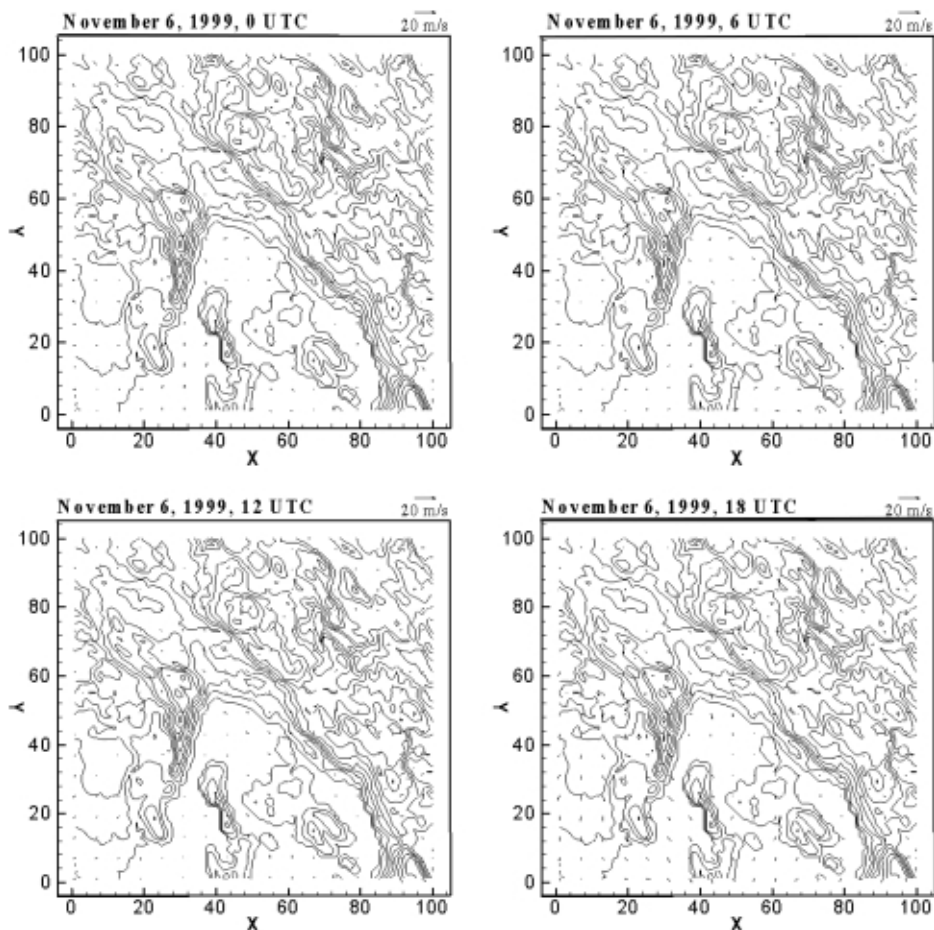


Figure 5. Modeled surface winds. Reference vector of magnitude of 20 m s^{-1} is indicated in the upper right corner. Wind vectors are shown at resolution of 6 km. Topography contours are given for every 200 m.

Bay. Throughout November 7, the wind speeds have increased and at 18 UTC the strongest winds over the Kvarner Bay exceeded 20 m s^{-1} . This is in agreement with findings of Makjanić (1970, 1976), who showed that, during the Bora, winds speeds are higher farther from the coastal barrier than on the coast itself. Furthermore, it reflects the fact that the airflow accelerates when it transitions from a rougher to a smoother surface (*i.e.* from the land to the sea).

Figure 6 shows the modeled wind fields for 6 and 7 November at 12 UTC at 1606, 3129 and 5104 m ASL. These heights were selected from the available model output levels as the closest to the typical heights of the 850, 700

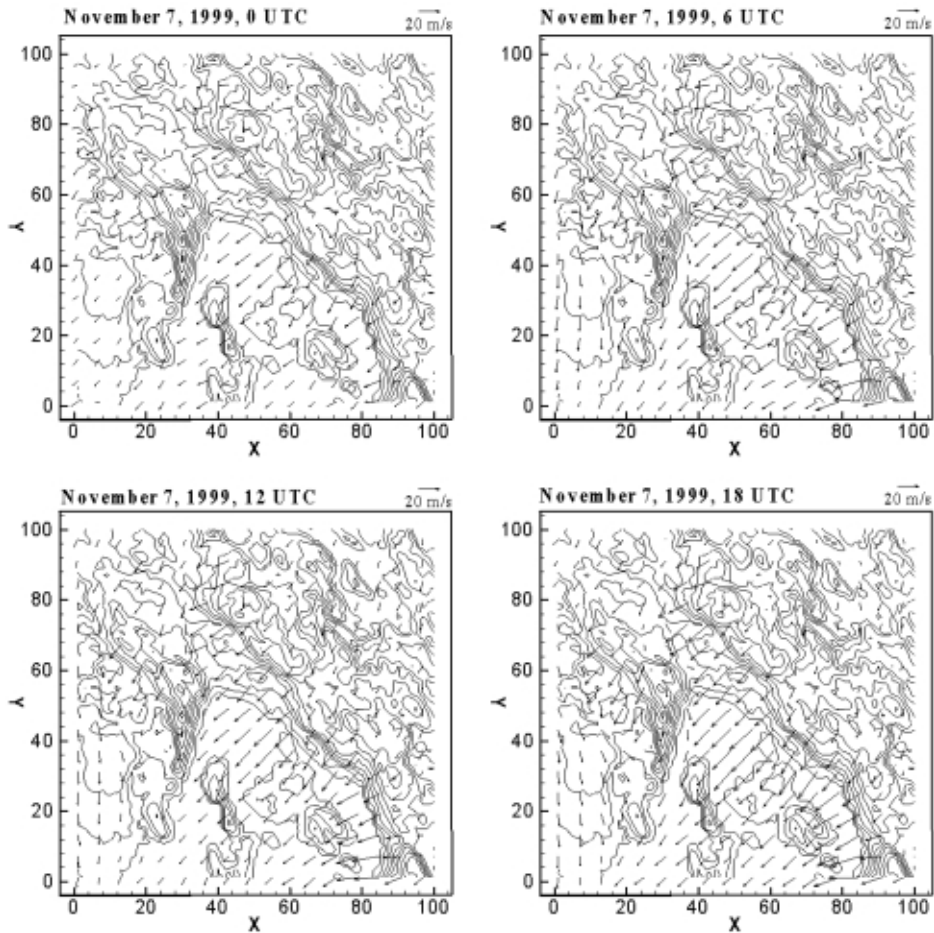


Figure 5. cont.

and 500 hPa isobaric surfaces. One may see that the modeled winds agree well with the corresponding upper-level diagnostic winds shown in Figure 2. The good agreement of both the wind direction and speed magnitudes at these upper-level surfaces further confirms our doubts about the accuracy of the measured surface winds at Rijeka and Senj shown in Figure 4.

5.1 Comparison with MAP measurements

On 7 November 1999 the NCAR Electra flight above the Adriatic, along the Croatian coast, was performed along tracks, which are parallel to and located 56.2 km southwestward (downwind) from the line AB. The Electra

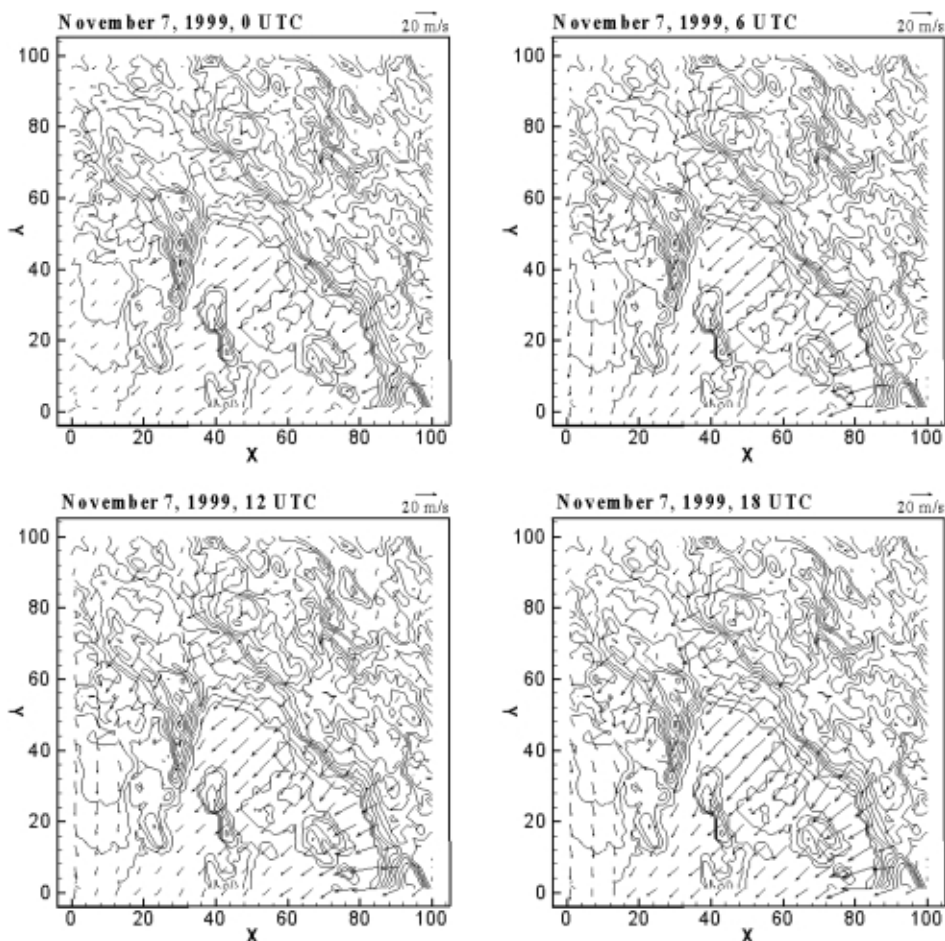


Figure 5. cont.

tracks, which lie entirely over the sea surface, come in close proximity of the southwestern corner of our domain (Figure 3). Although the aircraft tracks lie outside the domain of this study, the expectation is that, aside from the modifications induced by the Kvarner Bay islands (Krk and Cres) and the Istria Peninsula topography, the main features of this strong Bora would be comparable along the aircraft track and the line AB, especially along that portion of the line AB that lies over the sea. The first analyzed flight segment, which took place from 14:30 UTC to 15:01 UTC (where LST = UTC + 1), was flown at approximately 600 m ASL from the southeast to the northwest (*i.e.* parallel to the line BA). The second flight segment was flown in the opposite direction (*i.e.* parallel to the line AB) at about 300 m ASL, and, it lasted from 15:04 to 15:42 UTC. Consequently, we have investigated modeled

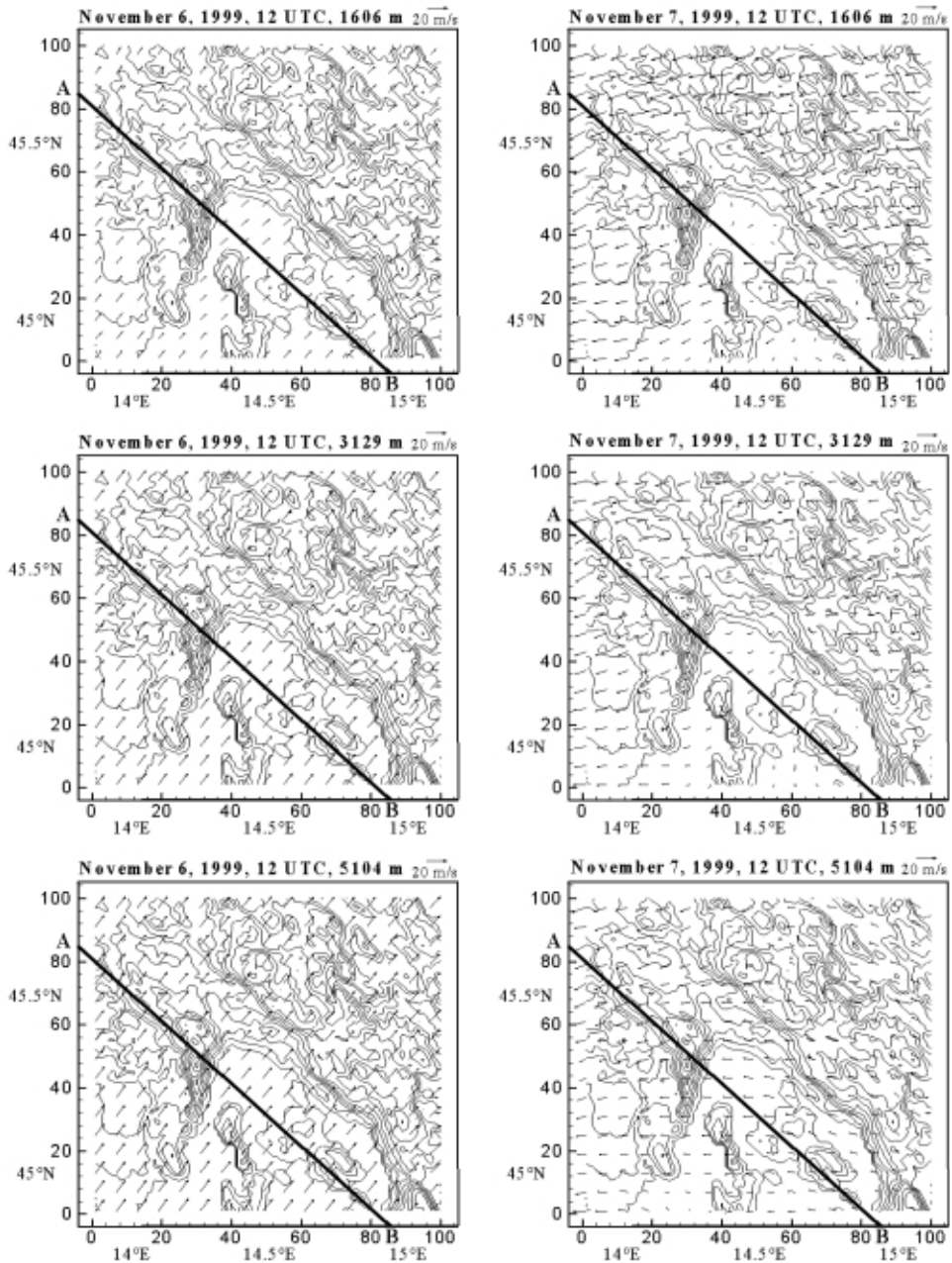


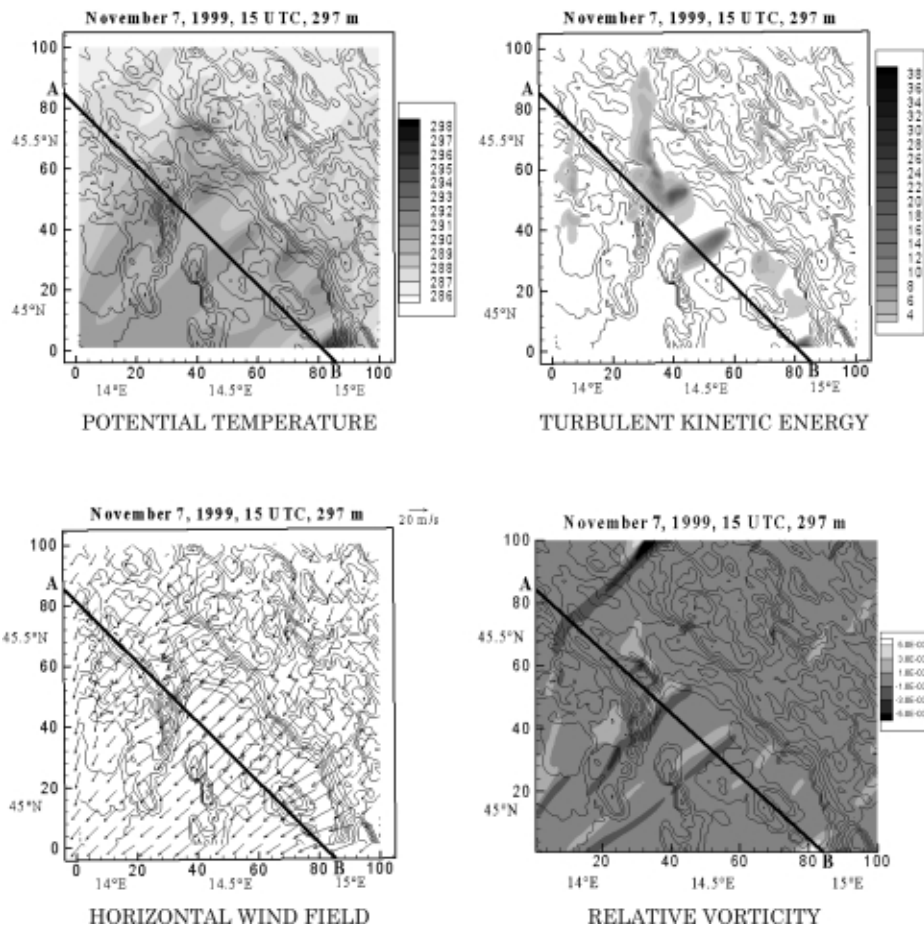
Figure 6. Modeled winds for 6 (left) and 7 (right) November 12 UTC at 1606, 3129 and 5104 m above the surface (top, center and bottom, respectively). Reference vector of magnitude of 20 m s⁻¹ is indicated in the upper right corner. Wind vectors are shown at resolution of 6 km. Topography contours are given for every 200 m.

θ , TKE , horizontal wind, and ζ fields at the model levels closest to the aircraft flight levels at 15 UTC (Figure 7). Note that the aircraft flight altitudes correspond to heights above the sea surface, whereas the model altitudes correspond to the heights above the terrain. For this analysis, we have selected the 297-m and 549-m model surfaces as the most suitable. Above the sea these terrain-following surfaces are at approximately the same heights as the Electra tracks, whereas over land, as revealed by track-perpendicular cross-sections (not shown here), these terrain-following surfaces are closely paralleled by isentropic surfaces.

As this MAP research flight was part of the Potential Vorticity (PV) banner project, whose aim was to investigate a complex horizontal structure of the wake generated by a major mountain range, we first take a look at the model predicted vertical vorticity (ζ) illustrated in Figure 7. Due to relatively small horizontal potential temperature gradients at the selected model surfaces away from the topography, the vertical vorticity is a good approximation for the PV there. As seen in Fig. 7, the model-predicted vorticity shows downstream-elongated filaments (banners) of vertical vorticity, which occurred in pairs of positive and negative vorticity downstream of the prominent topographic features, in good agreement with the MAP results (Grubišić, 2004). The absolute values of the model-predicted vertical vorticity (ζ) within the banners are on the order of 10^{-3} s^{-1} , and are slightly larger at the higher selected model surface. Furthermore, two regions in which vertical vorticity reaches 10^{-2} s^{-1} are found at both surfaces. One of these regions is within the filaments in the upper left corner of the domain, which are related to the flow around the southeastern edge of the Alps located in Slovenia. The other is located in the lower right corner, in the region of Senj, where a strong pair of vorticity banners forms. The horizontal dimensions of individual (positive or negative) filaments are a few tens of kilometers in the downstream direction, and a few kilometers in the direction perpendicular to the Bora flow. These model-generated vorticity banners are somewhat narrower than those documented in Grubišić (2004), where the characteristic width of the banners was 10–25 km. This difference in width of the vorticity banners is likely due to different horizontal resolutions at which the two models were run, and the known tendency for the numerically simulated PV banners to obtain finer spatial structure at higher model resolutions (Schär et al., 2003).

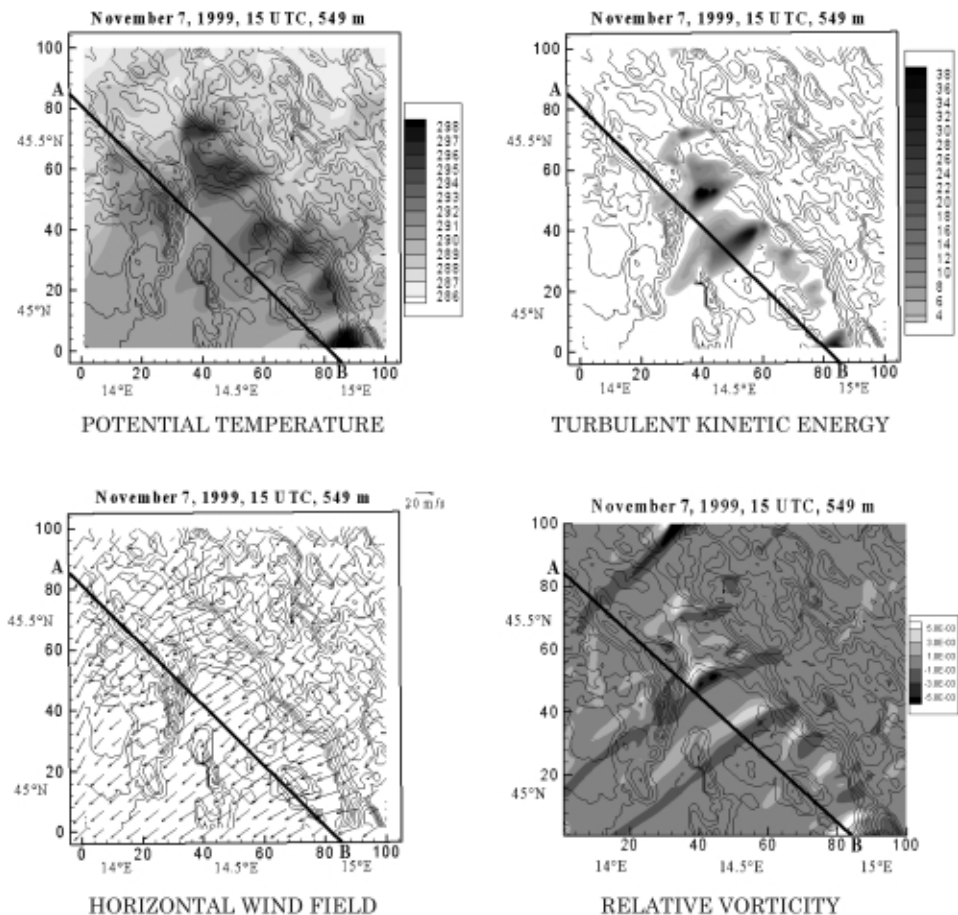
As further seen in Fig. 7, the origin of the pairs of vorticity (ζ) filaments coincide with the downwind-elongated areas of increased potential temperature and turbulent kinetic energy. Regions with the highest θ values are found downstream of the steepest mountain slopes, which is the consequence of (quasi-)adiabatic parcel heating in the strong katabatic flow. However, the increased TKE , together with the ζ anomalies, suggest that a topographically-induced irreversible transformation of approximately balanced synoptic-scale airflow to an unbalanced smaller-scale flow occurs in these zones.

The increased values of TKE are generally higher at the 549-m surface. On both the investigated surfaces there are three regions with particularly high TKE values. One of these regions is located to the west of Rijeka ($x \approx 44$ km, $y \approx 52$ km) at the northernmost tip of the Kvarner Bay, where at 15 UTC the maximum TKE of 47 and $22 \text{ m}^2 \text{ s}^{-2}$ was predicted at 549 and 297 m above the terrain, respectively. The second region of increased TKE is found about 15 km southward of Senj ($x \approx 85$, $y \approx 2$ km), where corresponding maximum TKE values are 43 and $33 \text{ m}^2 \text{ s}^{-2}$. The third region is located at $x \approx 58$ and $y \approx$



(a)

Figure 7. Modeled potential temperature (K), turbulent kinetic energy ($\text{m}^2 \text{ s}^{-2}$), horizontal wind field (m s^{-1}) and relative vorticity (s^{-1}) at 15 UTC at 297 and 549 m above the surface ((a) and (b), respectively).



(b)

Figure 7. cont.

38 km with TKE values of 37 and 17 $\text{m}^2 \text{s}^{-2}$. Similar TKE fields at both surfaces are also obtained for 14 UTC (not shown here).

Figure 8 shows the NW-SE vertical cross-section of the modeled θ , TKE , and the horizontal wind speed component perpendicular to the cross-section plane for 7 November 1999 at 15 UTC. The base of the cross-sections is line AB (*i.e.* it is about 56 km apart from the Electra track). Within the first ≈ 1.2 km above the ground over the Istria peninsula, isentropes are very densely spaced, with $\partial\theta/\partial z \approx 9.2 \text{ }^\circ\text{C km}^{-1}$, indicating strong static stability. Over the Island of Krk a less stable ($\partial\theta/\partial z \approx 5.0 \text{ }^\circ\text{C km}^{-1}$) but equally deep layer is found. Over the Kvarner Bay, the stable layer ($\partial\theta/\partial z \approx 8.0 \text{ }^\circ\text{C km}^{-1}$) is elevated, and extends from about 200 m up to about 700 m above the sea. A par-

ticularly strong stable layer ($\partial\theta/\partial z \approx 12.0 \text{ }^\circ\text{C km}^{-1}$), extending from the sea surface up to about 500 m ASL, is found above the point B, which is located about 15 km south of Senj.

Two shallow turbulent regions with $TKE > 18 \text{ m}^2 \text{ s}^{-2}$ are found in this vertical cross-section at 15 UTC (Fig. 8). The one above the Kvarner Bay starts at about 400 m ASL, and is approximately 6 km wide and 500–600 m deep. The other, south of Senj is of the same depth but located closer to the sea surface. Since this region is located at the very edge of the domain, its horizontal extent could not be determined. The relative contribution of shear-generated vs. buoyancy-generated turbulence, where the latter is due to the

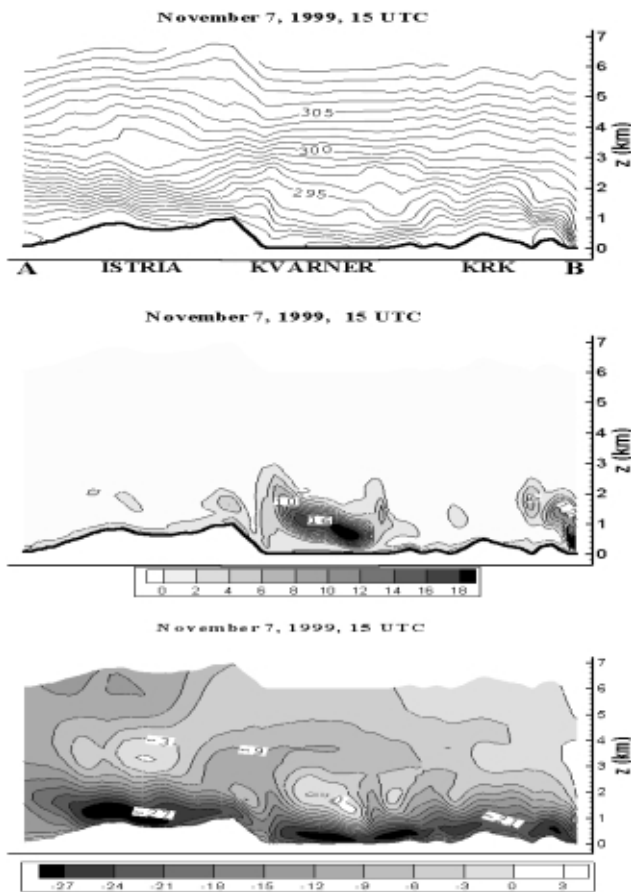


Figure 8. NW-SE vertical cross-section whose base is indicated with the line AB in Figure 3. Modelled values of potential temperature (K, top), turbulent kinetic energy ($\text{m}^2 \text{ s}^{-2}$, center) and horizontal wind speed component perpendicular to the cross-section (m s^{-1} , bottom) for 7 November 1999 15 UTC. Positive and negative wind speeds correspond to southwestern and northeastern flows, respectively. z is height above the sea level.

cold Bora wind flow over the warmer sea, remains yet to be determined. However, the strong static stability in these turbulent regions implies the importance of the shear generation mechanism.

The isotach cross-section, in which the wind component perpendicular to the cross-section plane (*i.e.* the along-Bora component) is shown, reveals that within the first few hundred meters above the surface the modeled wind speeds over the Istria Peninsula, the Kvarner Bay, and over the point B exceed 24 m s^{-1} . Above these wind speed maxima, within the first 1200–1600 m above the surface, a very strong wind shear is predicted, with values of $-1.8 \text{ m s}^{-1}/100 \text{ m}$, $-1.5 \text{ m s}^{-1}/100 \text{ m}$ and $-1.0 \text{ m s}^{-1}/100 \text{ m}$ corresponding to the Kvarner Bay, point B and Istria, respectively. The strong wind shear layer is deepest over the Istria, and the shallowest over the Kvarner bay. Further aloft, areas of weak northeasterly winds ($\leq 3 \text{ m s}^{-1}$), or even very weak southwesterly winds are found at altitudes between 2–3.5 km above the ground (over Istria) and 1.6–2.8 km above the sea (Kvarner Bay). In these 'calm' regions the vertical gradients of potential temperature are very small, with values of $\partial\theta/\partial z$ from 0.8 to $1.0 \text{ }^\circ\text{C km}^{-1}$.

The predicted multiple-maxima near-surface wind structure bears some resemblance to the Electra measurements for 7 November 1999 (Grubišić, 2004), which show a strong, cold, northeasterly jet over the Northern Adriatic, centered at 44.75°N , together with two more regions of increased wind speed at the northern and the southern end of the Electra track. At the height of 600 m ASL within a jet, a maximal measured wind speed perpendicular to the aircraft track (*i.e.* approximately perpendicular to the northern part of the Croatian coast) was close to 30 m s^{-1} .

Figures 9 and 10 show MAP measured vs. modeled winds, potential temperature, and the vertical component of relative vorticity derived from the measured and simulated winds. The vertical vorticity was computed from the Electra measurements following Grubišić (2001, 2004). In order to facilitate a direct comparison with the Electra data, the line AB and the data along it were translated in the downwind direction, parallel to the Bora flow, and projected onto the Electra flight track. The resulting uniform shift in the latitudes along the line AB is 0.36 degrees.

Since the model values, shown in Figs. 9 and 10 for 14 and 15 UTC, are taken along the 297-m and 549-m terrain-following surfaces along the line AB, the best agreement with the Electra measurement should be expected along the portion of the line AB that lies over the sea. This is indeed true for the horizontal and vertical wind speed components. On the other hand, the modeled wind direction agrees very well for the both heights along the entire line AB. Potential temperature discrepancy between the MAP measurements and modeled values, which is rather noticeable even above the sea, could be attributed to two factors: the MEMO model simplifications, and the distance between the Electra track and the line AB. Considering the first factor, one should note that the temporal variation of the sea surface temperature is ne-

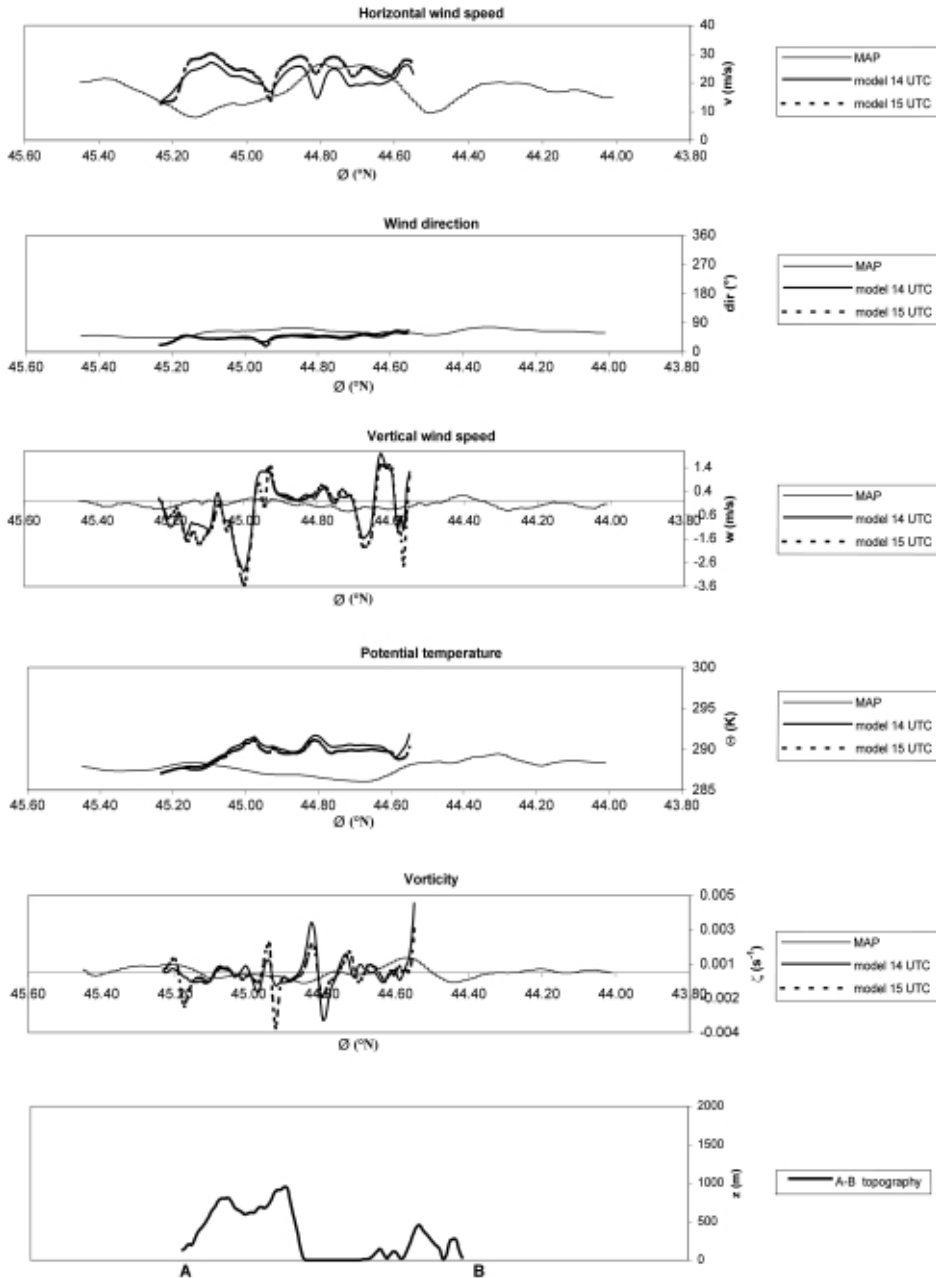


Figure 9. A comparison between the MAP measurement at ≈ 300 m above the sea level and the modeled values 297 m above the surface across the line AB (see Fig. 3) at 14 and 15 UTC. Abscissa Φ shows the latitude along the MAP flight track. This flight segment was flown from the higher to the lower latitude. In the lowermost panel, shown is the terrain height along the line AB.

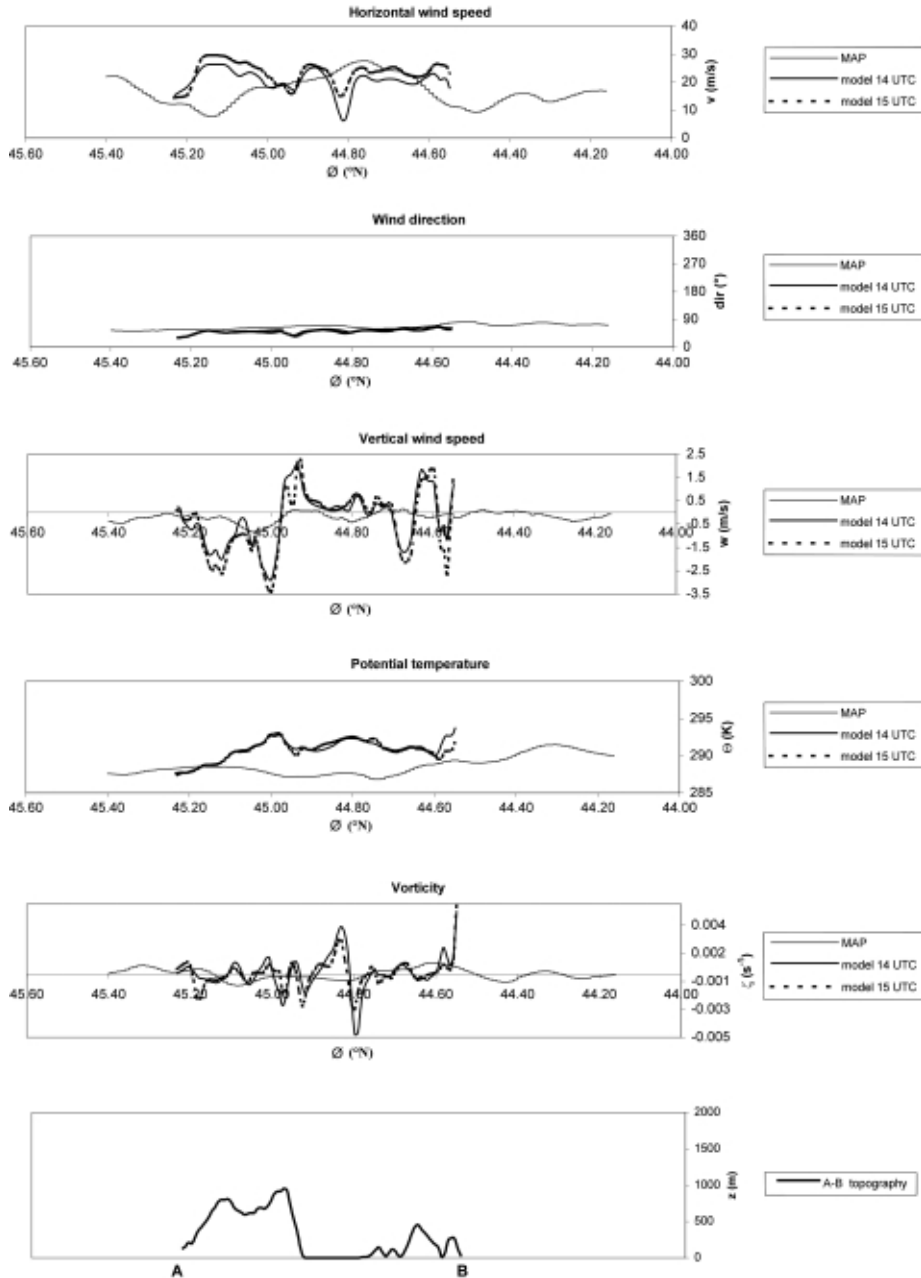


Figure 10. A comparison between the MAP measurement at ≈ 600 m above the sea level and the modeled values 549 m above the surface across the line BA (see Fig. 3) at 14 and 15 UTC. Abscissa Φ shows the latitude along the MAP flight track. This flight segment was flown from the lower to the higher latitude. In the lowermost panel, shown is the terrain height along the line AB.

glected in the MEMO model, while the temporal variation is taken into account for the ground surface temperature. Therefore, the modeled potential temperature, which is calculated from the surface heat balance equation, appears to agree better with the MAP measurements over the ground at low elevations than to measurements over the sea. The second factor, the distance between the Electra track and the line AB might be contributing even more to this discrepancy, with the line AB being much closer to the topography and the zones of strong katabatic heating.

5.2 Temporal development of flow in the Senj region

In this section we examine in more detail the model results for the Senj region. Figures 11, 12 and 13 show the west-east vertical cross-sections through Senj for wind, potential temperature and turbulent kinetic energy fields for 6–7 November 1999. These west-east oriented vertical cross-sections are the along-Bora sections since the wind direction in Senj and its surrounding during this Bora event is easterly. As illustrated in Figure 11, until 6 November at 23 UTC winds were weak and westerly. The wind speed exhibited the expected increase with height due to the attenuation of frictional effects. After 23 UTC on November 6, the zonal flow reversed to the easterly. Simultaneously, the wind speed at lower levels (*i.e.* within the Bora layer, defined here as the layer with strong winds $\geq 10 \text{ m s}^{-1}$ and the easterly Bora direction, characteristic of Senj) became stronger than the winds aloft, and, due to the severe downslope nature of the flow, continued to increase with time. At the beginning of the Bora period (23 UTC on November 6), the horizontal and vertical wind components within the Bora layer in the Senj region were close to 20 m s^{-1} and -2 m s^{-1} , respectively. At the end of simulated period (22 UTC on November 7), corresponding numbers were about 30 m s^{-1} and -4 m s^{-1} . The Bora wind was strongest within approximately first 2 km above the surface. The depth of the Bora layer in these cross-sections is larger upwind of the mountain crest ($\sim 2 \text{ km}$) compared to the mountain slope and the zone over the sea in between the Senj and the Island of Krk ($\sim 1 \text{ km}$). The latter is in good agreement with the depth of the Bora layer determined from the MAP Electra lidar measurements (Grubišić, 2004).

The modeled Bora event produced a hydraulic-jump-like feature over the coastal mountain slopes, which is clearly evident in the potential temperature cross-sections (Figure 12) at the height of 1.5 to 2 km. At the downstream end of the jump, located over the sea in between Senj (on the coast) and the Krk island, the vertical wind component was strongly positive, further confirming the presence of a hydraulic jump. This feature is located well upstream of the islands and at an altitude at which it is clearly distinguishable from the upward motions due to the flow over island topography.

The temporal development of the potential temperature field in the same cross-section is shown in Figure 12. At 05 UTC on November 6 the lower tro-

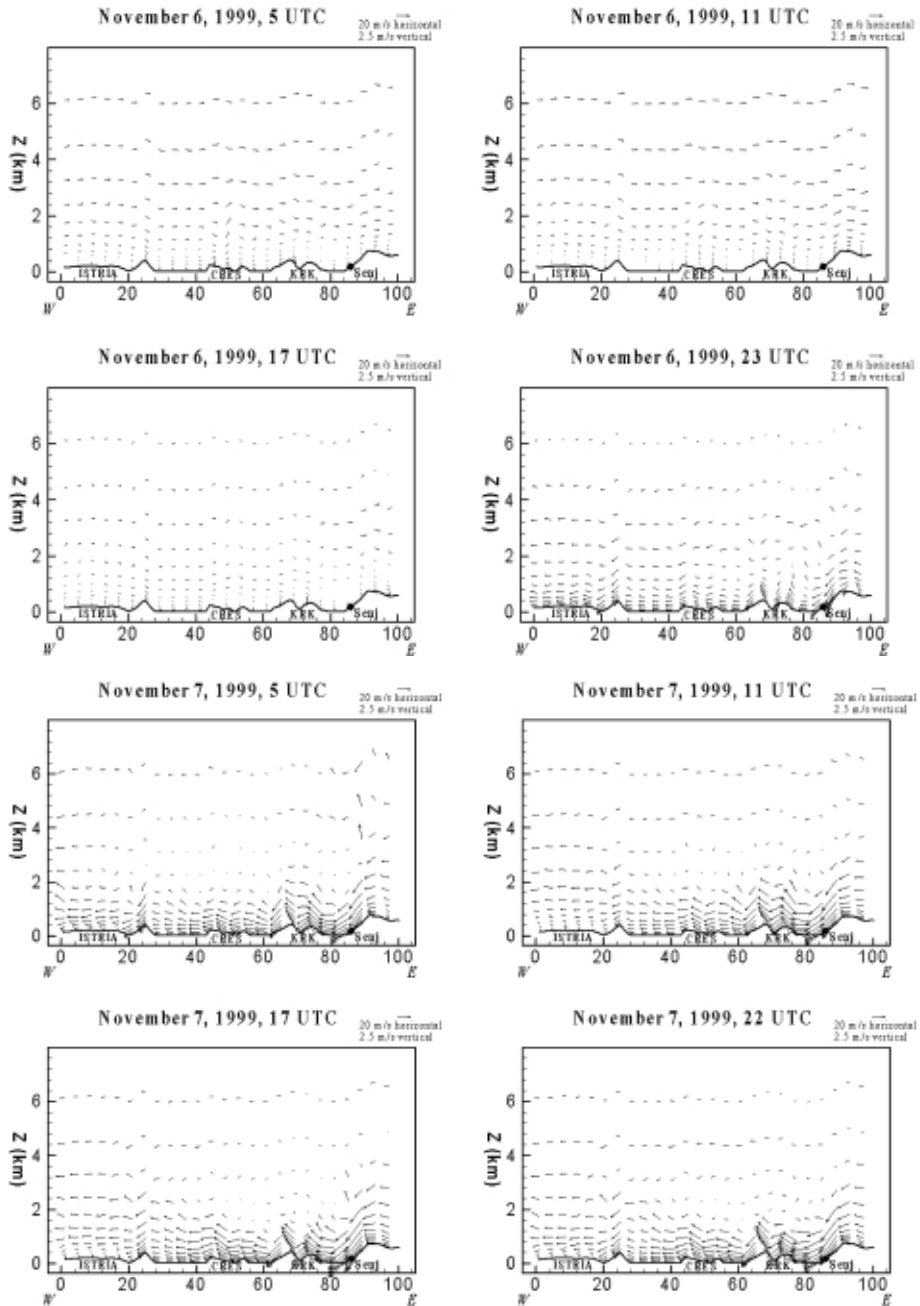


Figure 11. West-east vertical cross-section of the modeled winds for Senj (position of Senj is indicated with the circle). Wind vectors shown are vector sums of the modeled eastward and vertical wind components.

posphere was statically stable, with spatially uniform stability. The potential temperature field did not change significantly until 11 UTC on November 6, when a less stable layer started forming within the first 2 km above the surface. This layer of weak static stability was covered with a more stable layer, extending from about 2.8 km to 4.4 km.

At 17 UTC on November 6, the static stability of the lowest portion of the atmosphere across the entire cross-section was further decreased. The rising of the isentropes upstream (eastward) of the ridge is clearly seen, with this layer of upward flow extending up to 2 km above the ground. At this time, there is also an indication of the downslope flow initiation over the ridge. Six hours later, at 23 UTC on November 6, a dense packing of isentropes above Senj clearly suggests flow acceleration in this region of strong static stability ($\partial\theta/\partial z \sim 2 \text{ K}/100 \text{ m}$) together with the attendant hydraulic jump at the downstream end. It is also apparent that the acceleration of Bora flow starts upwind of the mountain crest as indicated by the downward sloping isentropes there. With time, the descending isentropes above the mountain slope became more densely packed (compare, for example, 7 November 11 UTC with 17 and 22 UTC), and occupy a deeper layer. This suggests the deepening of the Bora layer and the intensification of acceleration, *i.e.* the strengthening of the Bora wind, the latter being confirmed by observations. Significant deformations of isentropes are also found downstream of the Krk and Cres as well as the eastern Istria topographic barriers, especially during the early development stage of this Bora (5 UTC November 7). However, since these obstacles are lower than the coastal range, the hydraulic jumps they produced were not as intense as the one in the Senj region. Later in this Bora development, only the hydraulic jump in the Senj region and the large isentropic deformations downwind of Krk remained.

Finally, Figure 13 shows the cross-sections of the modeled *TKE*. The weak turbulence ($\sim 1 \text{ m}^2 \text{ s}^{-2}$) started developing sporadically in the lowest layers only after 17 UTC on 6 November. At 5 UTC on November 7 turbulent regions were located downstream of topographical obstacles with the maximal values about 1.4 km above the ground. The highest values (up to $14 \text{ m}^2 \text{ s}^{-2}$) are found in the Senj region, whereas downstream of Krk, Cres and the Istrian coast values up to 7, 4, and $2 \text{ m}^2 \text{ s}^{-2}$ are found, respectively. It should be noted that in our diagrams these regions are vertically stretched, and that their horizontal and vertical dimensions are $\sim 10 \text{ km}$ and $\sim 1 \text{ km}$, respectively. With time, the regions of maximum *TKE* moved slowly downstream with the turbulence downstream of Krk intensifying more strongly compared to the Senj region. At 17 UTC on November 7 the maximal predicted values of *TKE* downstream of Krk and Senj were 30 and $13 \text{ m}^2 \text{ s}^{-2}$, whereas at 22 UTC on November 7 the corresponding numbers were 21 and $18 \text{ m}^2 \text{ s}^{-2}$, respectively. A comparison of Figures 12 and 13 shows that the regions of maximal *TKE* values coincide with the large deformation of isentropes within the hydraulic jump regions.

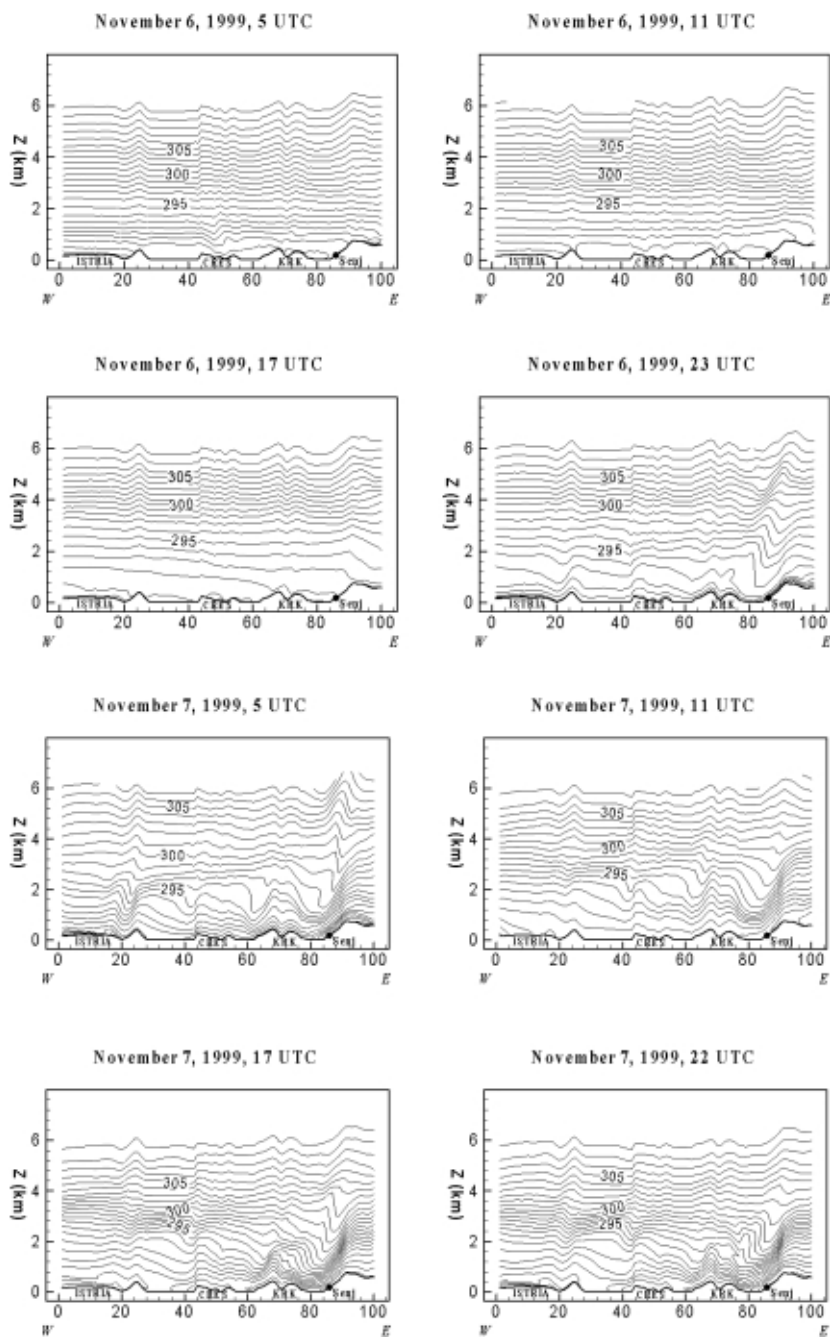


Figure 12. West-east vertical cross-section of the modeled potential temperature (K) for Senj (position of Senj is indicated with the circle).

5.3 Hydraulic flow: Further details

Since the model results for the Senj region revealed the presence of interesting hydraulic-like airflow features with what appear to be multiple hydraulic jumps, in this section we shall further investigate the evolution and properties of this flow. In the seminal papers by Long (1953, 1954), the foundations of the hydraulic flow analogy were laid out for a class of stratified airflows over an obstacle. In the first paper (1953), the author gave a theoretical analysis of the formation of a »hydraulic jump« in the stratified flow, whereas in the latter study (1954) he described several laboratory experiments with a two-fluid system. In discussing meteorological implications, Long pointed out that a hydraulic jump is expected to form in the lee of an obstacle if the internal Froude number (Fr) exceeds a certain value, depending on the height of an inversion (defining a top of the hydraulic layer) and the height of the obstacle. The internal Froude number is $Fr = U / N h$, where $N = (g \theta^{-1}) \partial\theta/\partial z$ is the Brunt-Väisälä frequency, U is the mean wind speed, and h is the mountain top height. Nonlinear effects in the stratified fluid flow over two-dimensional sinusoidal topography were investigated analytically by Smith (1977). According to his results, the nonlinear effects are important for moderate and large mountains (whenever non-dimensional mountain

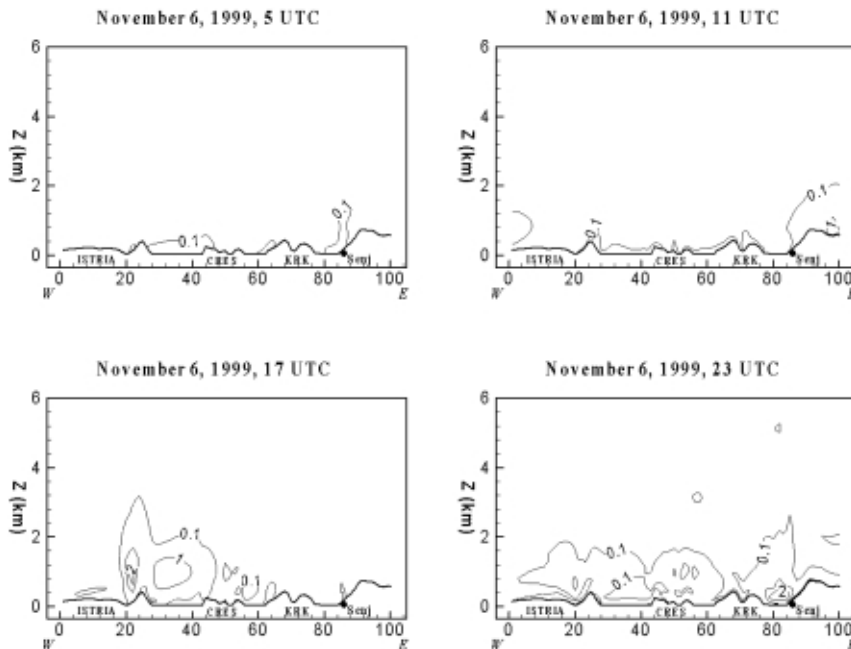


Figure 13. West-east vertical cross-section of the modeled turbulent kinetic energy ($\text{m}^2 \text{s}^{-2}$) for Senj (position of Senj is indicated with the circle).

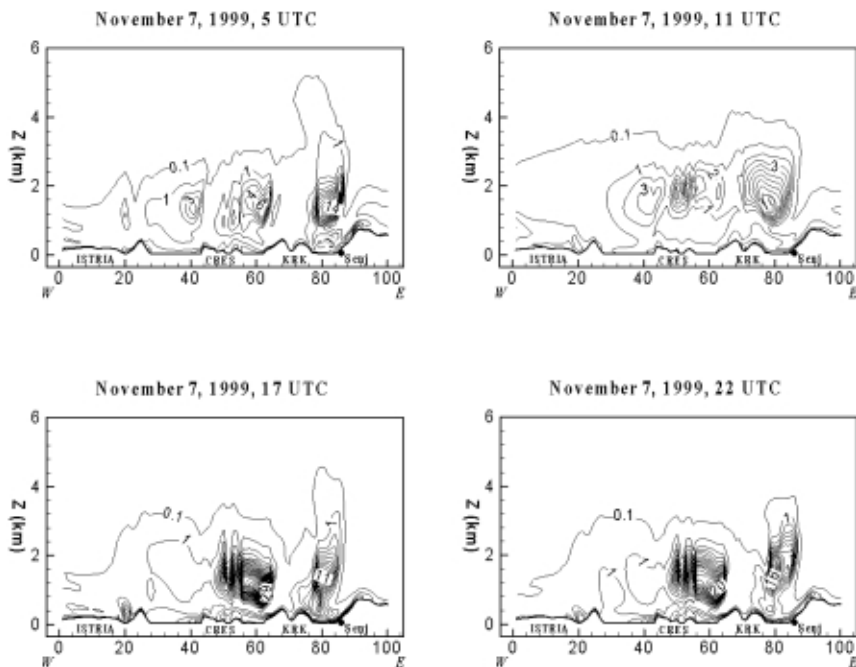


Figure 13. cont.

height Nh/U , which is equal to Fr^{-1} , approaches 1) even when mountain slopes are very gentle. Furthermore, Smith pointed out that the nonlinear lower-boundary condition has an important influence on the production of severe downslope winds. Based on idealized 2-D numerical simulations, Durran (1986) showed for case when the static stability has a two-layer structure and the parameter Nh/U is as small as 0.3, that i) nonlinear waves are much larger than their linear counterparts, ii) the highest stability is found in the lower layer, and iii) that the flow resembles a hydraulic jump. Durran's simulation results for the Boulder windstorm, which according to Smith (1987) is dynamically similar to the Bora, suggest that the transition to supercritical flow (*i.e.* flow with $Fr > 1$), forced by the presence of a low-level inversion, plays an essential role in triggering the windstorm.

For a further investigation of the hydraulic nature of the Bora flow, we have selected an along-Bora vertical cross-section whose base is shown in Fig. 3 as line CD. Compared to the E-W vertical cross-sections for Senj (Figs. 11–13), the CD section extends substantially further eastward over the mainland. Along line CD we have marked points 1–7, which are indicated in Fig. 3, as well as in the vertical cross-sections in Figures 14–16. These points are selected as representative of conditions over the mainland (1 and 2), downstream of the coastal mountains (3), at the top of the islands (Krk and Cres)

(4 and 6), in the channel between the two islands (5), and on the lee side of the last obstacle (7). Figures 14–16 show the modeled wind, potential temperature, and turbulent kinetic energy fields.

As seen from Figures 14–16, strengthening of the Bora is accompanied with the increase of static stability in the lower part of the atmosphere (Fig. 15 for November 7, for times from 09 to 18 UTC). This lowermost statically

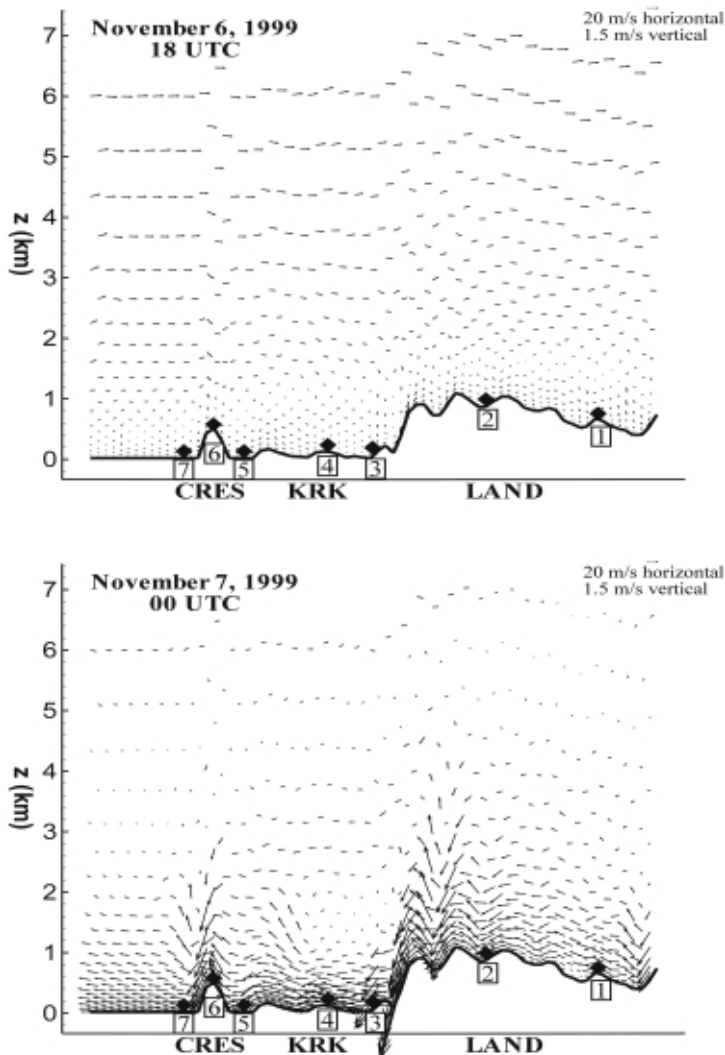


Figure 14. NE-SW vertical cross-section of the modeled winds. The base of the cross-section (line CD) and the locations of points 1–7 are indicated in the Fig. 3. NE and SW are at the right and left side of the figure, respectively.

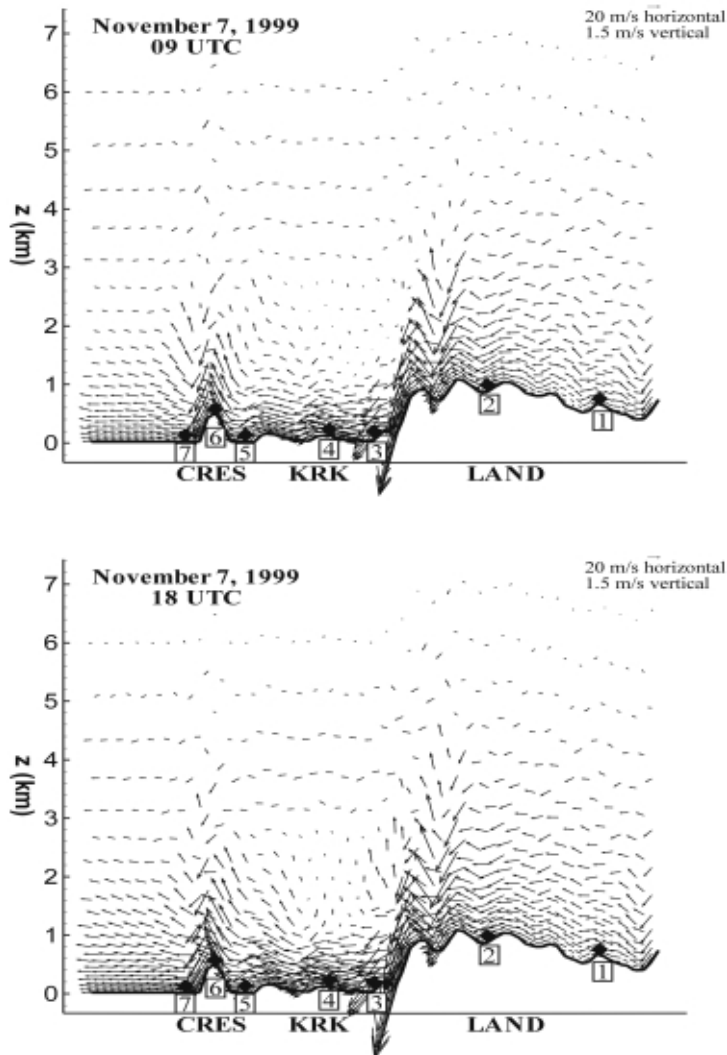


Figure 14. cont.

stable layer is deeper over the mainland than downstream of the mountains: above point 1 (over the mainland) the depth of the statically stable layer is about 3 km, while above points 3 and 4 (over the sea) this layer is about 1 km deep. The static stability is strongest above the major lee slope adjacent to the sea (a few km northeastward from point 3), where on November 7 at 18 UTC the model predicted $\partial\theta/\partial z \sim 1.2$ K/100 m. (At that same time, in the most statically stable region above Senj $\partial\theta/\partial z \sim 1.6$ K/100 m.) Downstream of the

coastal mountains, a rather deep (≈ 2 km) mixed layer is formed above this very stable lowest layer with strong winds. Within this mixed layer, characterized with a weak vertical potential temperature gradient and weak winds, isolated regions of high TKE are found (compare Figs. 14–16).

Additional examination of conditions along the line CD (not shown here) confirms the presence of a cold-air outbreak, in accordance with the study of Bajić (1987). This cold-air outbreak is more pronounced at the windward side of the mountains. For example, the modeled surface temperature for the end points 1 and 7 decreased, respectively, about 5 and 2 K from November 6 at 18 UTC to November 7 at 18 UTC. This indicates the damming of cold air upstream of the coastal mountains, and build up of upstream fluid stratification.

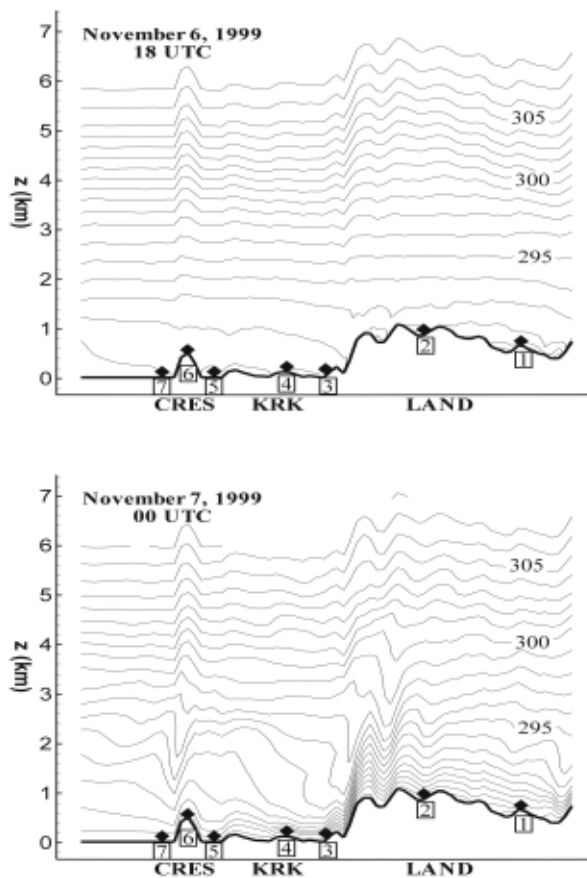


Figure 15. NE-SW vertical cross-section of the modeled potential temperature (K). The base of the cross-section is indicated in the Fig. 3 by the line CD. NE and SW are at the right and left side of the figure, respectively.

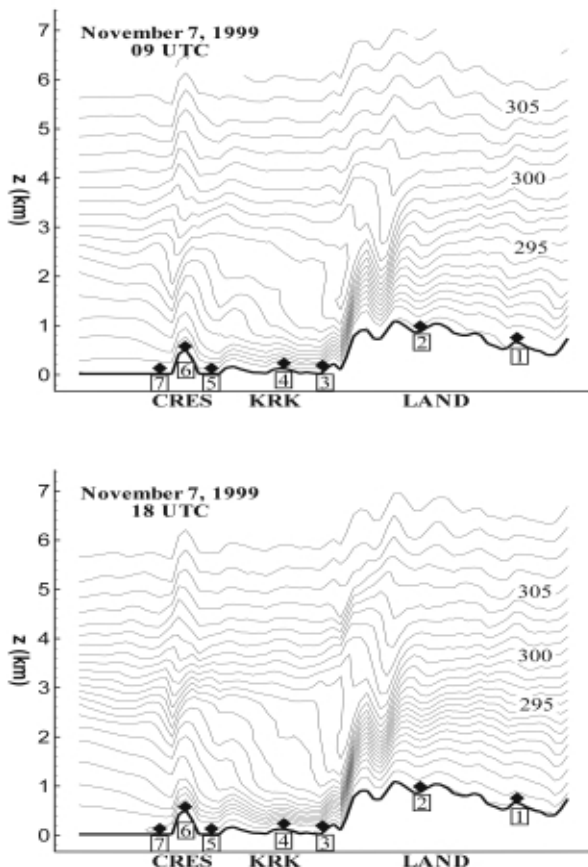


Figure 15. cont.

Table 1 shows values of the Froude number (Fr), Brunt-Väisälä frequency (N), and along-Bora mean wind speed component (U) within the Bora layer for the seven points along line CD. Listed results clearly illustrate a temporal transition of the flow from a subcritical ($Fr < 1$) to a supercritical ($Fr > 1$) flow for all points apart from point 1, which is located about 40 km inland from the coastline. The transition was most rapid at point 3, *i.e.* at in the immediate lee of the coastal mountains. Furthermore, at the end of the investigated time period, at this point Fr reaches the highest value (1.75) compared to all other points along line CD. On the other hand, the transition from the subcritical to the supercritical flow was the slowest at point 2, where on November 7 at 18 UTC Fr was only slightly greater than the threshold value (1.02).

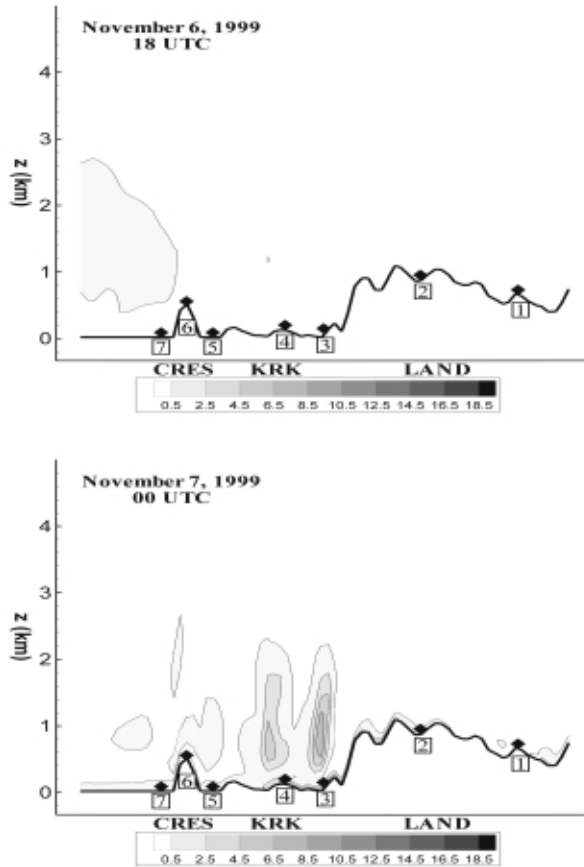


Figure 16. NE-SW vertical cross-section of the modeled turbulent kinetic energy ($m^2 s^{-2}$). The base of the cross-section is indicated in the Fig. 3 by the line CD. NE and SW are at the right and left side of the figure, respectively.

The model-derived Brunt-Väisälä frequencies (N) show a temporal increase of static stability at all seven points. The increase in N over the examined 24-hour interval is largest at points 1, 4, 6, where $\Delta N/\Delta t = 0.004 s^{-1} / 24 h$. This could be attributed to a denser packing of isentropes above the topographical obstacles. On the other hand, $\Delta N/\Delta t$ is the smallest ($0.002 s^{-1} / 24 h$) for points 5 and 7, which are located on the lee sides of the islands Krk and Cres, respectively. The largest static stability at the end of investigated period is found over the mainland ($N = 0.013 s^{-1}$, points 1 and 2), which further confirms stratification of the atmosphere upstream of the mountains due to the cold air damming.

Finally, throughout the whole Bora event modeled wind speeds were strongest downstream of the coastal mountains (point 3). On the other hand,

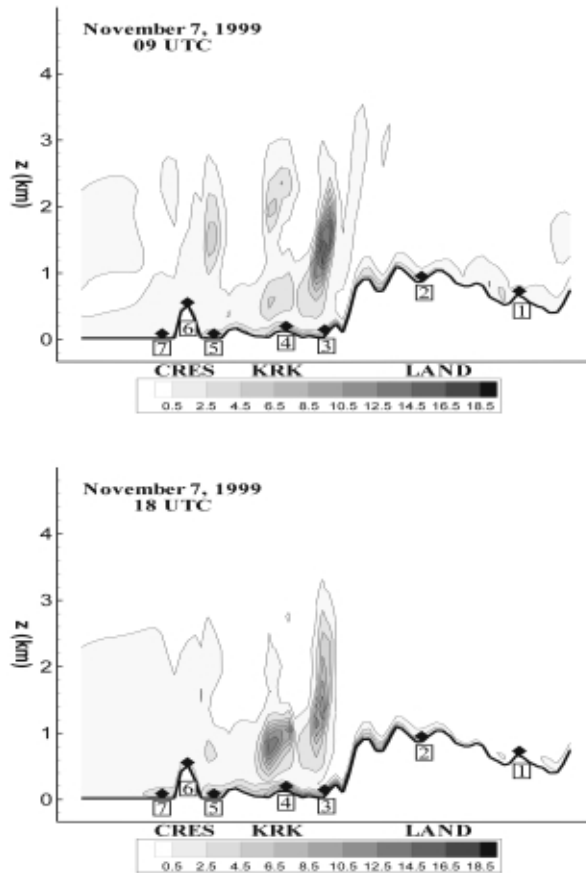


Figure 16. cont.

Table 1. Froude number ($Fr = U/Nh$), Brunt-Väisälä frequency N (s^{-1}) and along-Bora mean wind speed component U ($m s^{-1}$) within the Bora layer at points 1–7. Point positions are shown in Fig. 3 and Figs. 14–16.

Point	Nov. 7, 00 UTC			Nov. 7, 09 UTC			Nov. 7, 18 UTC		
	Fr	N	U	Fr	N	U	Fr	N	U
1	0.69	0.012	9.3	0.80	0.011	9.9	0.78	0.013	11.4
2	0.75	0.013	10.4	0.97	0.012	12.9	1.02	0.013	15.0
3	1.32	0.011	15.7	1.15	0.011	18.7	1.75	0.012	23.5
4	1.17	0.011	14.0	1.45	0.011	17.3	1.53	0.012	20.3
5	1.21	0.010	12.8	1.25	0.010	13.3	1.64	0.010	18.4
6	1.26	0.010	13.8	1.20	0.011	14.6	1.55	0.012	20.6
7	1.19	0.009	11.4	1.33	0.009	13.0	1.67	0.010	17.6

weakest wind speeds were predicted for the inland point 1, where throughout the whole Bora event airflow remained subcritical.

6. Conclusions

We have carried out a study of the 7 November 1999 Bora case employing the mesoscale nonhydrostatic model MEMO. The model was run over a relatively small domain but at a very high horizontal resolution (grid spacing of 1 km), which has afforded us a detailed insight in the meteorological conditions in the lower troposphere during the Bora event over the Northern Adriatic. The selected Bora case, one of the strongest Bora cases in recent decades, was documented during the Mesoscale Alpine Programme SOP (IOP 15) with in situ aircraft measurements over the Adriatic Sea. Additionally, we have used standard surface meteorological measurements available at several coastal sites as well as upper-level data for the model verification.

A comparison between the measured and the modeled surface winds for this Bora event showed that the employed mesoscale model was able to predict well both the wind directions and the timing of the Bora event. A good agreement was also found between the modeled and measured upper-level winds. Consequently, we found the large discrepancies between the measured and modeled surface wind speeds at Senj and Rijeka surprising. After further investigation and the consultation with the Meteorological and Hydrological Service of Croatia staff, we have reached the conclusion that the quality of Senj and Rijeka measurements is questionable due to the sheltered location of these two sites. In order to further investigate this data quality problem, in the future we plan to simulate Bora events from other time periods. One such period is the experimental period from December 2001 to January 2002, during which surface winds in Senj were measured at two measuring sites, the routine station used in this study as well as an additional experimental measuring site.

The comparison of our model results with the MAP IOP 15 measurements showed a good agreement. The model simulation reproduced the topographically induced elongated relative vorticity filaments, whose downstream lengths and widths perpendicular to the airflow were a few tens of kilometers and a few kilometers, respectively. We note, however, that the full length of the vorticity banners is likely much larger, and could not be captured in our relatively small domain. Also, the width of the vorticity banners was smaller than measured in MAP and simulated by the COAMPS model at the resolution of 3 km. This seems to point to a known tendency of simulated vorticity banners to display finer structure at higher model resolutions. The maximum value of the vertical vorticity (ζ) within the anomalies was on the order of 10^{-2} s^{-1} . The origin of vertical vorticity anomalies coincided with the downstream-elongated regions of increased potential temperature (θ) and turbu-

lent kinetic energy (*TKE*). The latter, together with the vorticity anomalies indicate regions of irreversible transformation of the balanced synoptic scale flow to the smaller scale unbalanced airflow.

The examination of the along-Bora vertical cross-sections showed a formation of the ground-based layer of strong static stability. This stable layer was much deeper over the mainland (≈ 3 km) compared to the layer downwind of the mountains, where its depth (≈ 1 km) was comparable with the height of the coastal mountains. The strongest static stability, on the order of magnitude of $\partial\theta/\partial z$ of 1 K/100 m, was found above the major lee slope adjacent to the sea.

Downstream of the coastal range, the maximal wind speeds (up to 30 m s⁻¹) were simulated. These zones of both the maximum low-level winds and strong static stability were capped with a rather deep (≈ 2 km) well-mixed layer of weak winds, which is in accordance with the results of Smith (1987). Therefore, a strong vertical wind shear (up to -1.8 m s⁻¹/100 m) was established. Regions of the strongest wind shear coincided with the horizontally extended regions of increased *TKE*, which indicates the importance of the shear generation of turbulent kinetic energy. The above *TKE* zones, of the horizontal and vertical dimensions of the order of magnitude of 10 and 1 km, respectively, were found downwind of the coastal mountains and the Island of Krk throughout the whole duration of the Bora event.

The model also captured well the transition over the mountains from a subcritical to a supercritical flow, which was forced by the blocking of the cold air upstream of the coastal mountains in the presence of a low-level inversion. The subsequent formation of multiple hydraulic jumps was also captured by the model. The strongest jump was associated with the highest portion of the coastal mountains (*i.e.* the highest topographical obstacle), where the most rapid transition from the subcritical to the supercritical flow, and the highest values of the Froude number (*Fr*) were predicted. Similar, but weaker jumps were found downstream of the islands. The zones of maximum *TKE* coincided with the regions of steeply rising isentropes within the hydraulic jumps.

Finally, we note that all investigated physical quantities exhibited their most dramatic temporal behavior and spatial gradients in the region of Senj.

Acknowledgements – We thank Theodoros Nitis of the Laboratory of Heat Transfer and Environmental Engineering, Aristotle University Thessaloniki, Greece for preparing the land-use and topography data. The standard meteorological data was kindly provided by the Meteorological and Hydrological Service of Croatia with a particular engagement of Dr. Branka Ivančan-Picek and Živko Trošić, M.Sc. Dr. Vanda Grubišić's involvement in this study was supported by the NSF grant ATM-0002735. We extend our thanks to the PV banner project scientists Christoph Schär, Louisa Nance, and Marty Ralph for their contributions in designing this PV banner mission and collecting the data, and numerous people within the MAP organization for making the MAP data used in this study available. This study was partially supported by the Ministry of Science and Technology of Republic of Croatia project no. 0119330.

References

- Bajić, A., (1987): Cold air outbreak and the Adriatic bora. *Geofizika*, **4**, 27–37.
- Bajić, A., (1991): Application of the two-layer hydraulic theory on the severe Northern Adriatic bora. *Meteorol. Rund.*, **44**, 129–133.
- Carpenter, K. M. (1982): Note on the paper 'Radiational condition for the lateral boundaries of limited-area numerical models' by Miller M. J. and Thorpe, A. J. (*Q. J. R. Met. Soc.*, **107**, 615–628). *Quart. J. R. Met. Soc.*, **108**, 717–719.
- Durran, D. E. (1986): Another look at downslope windstorms. Part I: The development of analogs to supercritical flow in an infinitely deep, continuously stratified fluid. *J. Atmos. Sci.*, **43**, 2527–2543.
- Enger, L., and Grisogono, B. (1998): The response of bora type flow to sea surface temperature. *Q. J. R. Meteorol. Soc.*, **124**, 1227–1244.
- Grubišić, V., (1989): Application of the hydraulic theory in cases of bora with strong upstream flow. *Rasprave*, **24**, 21–27.
- Grubišić, V., (2000): Bora driven PV banners over the Adriatic: Preliminary results. *MAP Newsletter* **13**, 66–67.
- Grubišić, V. (2001): Structure of wake north of the Alps: PV banners during an episode of deep south Foehn. *Proceedings. AMS Ninth Conference on Mesoscale Processes*, 30 July-2 August 2001, Ft. Lauderdale, FL, AMS, 180–183.
- Grubišić, V. (2004): Bora driven potential vorticity banners over the Adriatic. *Q. J. R. Meteorol. Soc.*, in press.
- Heimann, D., (2001): Model-based wind climatology of the eastern Adriatic coast. *Meteorol. Z.*, **10**, 5–16.
- Ivančan-Picek, B., and Tutiš, V. (1996): A case study of a severe Adriatic bora on 28 December 1992. *Tellus*, **48A**, 357–367.
- Jurčec, V. (1981): On mesoscale characteristics of bora conditions in Yugoslavia. *Pure Appl. Geophys.*, **119**, 640–657.
- Klaić, Z. B., and Nitis, T. (2001–2002): Application of mesoscale model (MEMO) to the greater Zagreb area during summertime anticyclonic weather conditions. *Geofizika*, **18–19**, 31–43.
- Klaić, Z. B., Nitis, T., Kos, I., and Moussiopoulos, N. (2002): Modification of the local winds due to hypothetical urbanization of the Zagreb surroundings. *Meteorol. Atmos. Phys.*, **79**, 1–12.
- Klaić, Z. B., Belušić, D., Herceg Bulić, I., and Hrust, L. (2003): Mesoscale modelling of meteorological conditions in the lower troposphere during a winter stratospheric ozone intrusion over Zagreb, Croatia. *J. Geophys. Res.-Atmos.*, **108**, 4720, 10.1029/2003JD003878J.
- Koračin, D. (1984): Parameters of bora flow. *Zbornik Meteorol. Hidrol. Radova*, **10**, 109–111.
- Kunz, R., and Moussiopoulos N. (1995): Simulation of the wind field in Athens using refined boundary conditions. *Atmos. Environ.*, **29**, 3575–3591.
- Lazić, L., and Tošić, I. (1998): A real data simulation of the Adriatic bora and the impact of mountain height on bora trajectories. *Meteorol. Atmos. Phys.*, **66**, 143–155.
- Long, R.R. (1953): Some aspects of the flow of stratified fluids. I. A theoretical investigation. *Tellus*, **5**, 42–58.
- Long, R.R. (1954): Some aspects of the flow of stratified fluids. II. Experiments with a two-fluid system. *Tellus*, **6**, 97–115.
- Makjanić, B. (1970): On the diurnal variation of the bora wind speed. *Papers*, **349**, Yugoslav Academy of Sciences and Arts, Zagreb, 33–92.
- Makjanić, B. (1976): A short account of the climate of the town Senj. In: *Local wind bora*. (Yoshino M. M., ed.), University of Tokio Press, 145–152.
- Makjanić, B. (1978): *Bura, jugo, etezija*. Prilozi poznavanju vremena i klime SFRJ. Svezak 5, Savezni hidrometeorološki zavod. Beograd.

- Moussiopoulos, N. (ed.) (1994): *The EUMAC Zooming model: model structure and applications*. Garmish-Partenkirchen: EUROTRAC special publication, ISS, 266 pp.
- Moussiopoulos, N. (1995): The EUMAC Zooming model, a tool for local-to-regional air quality studies. *Meteorol. Atmos. Phys.*, **57**, 115–133.
- Moussiopoulos, N., Sahm, P., Karatzas, K., Papalexioiu, S., and Karagiannidis, A. (1997a): Assessing the impact of the new Athens airport to urban air quality with contemporary air pollution models. *Atmos. Environ.*, **31**, 1497–1511.
- Moussiopoulos, N., Sahm, P., Kunz, R., Vögele, T., Schneider, C., and Kessler C. (1997b): High-resolution simulations of the wind flow and the ozone formation during the Heilbronn ozone experiment. *Atmos. Environ.*, **31**, 3177–3186.
- Orlić, M., Kuzmić, M., and Pasarić, Z. (1994): Response of the Adriatic Sea to the bora and sirocco forcing. *Continental Shelf Res.*, **14**, 91–116.
- Petkovšek, Z. (1990): Upper boundary of the bora as a stationary frontal surface. *Meteorol. Atmos. Phys.*, **43**, 197–202.
- Petkovšek, Z. (1991): Additional bora characteristics according to the frontal model. *Geofizika*, **8**, 25–31.
- Qian, M. W., and Giraud, C. (2000): A preliminary numerical simulation of bora wind with a limited area model of atmospheric circulation. *Nuovo Cimento Soc. Ital. Fis. C-Geophys. Space Phys.*, **23**, 515–523.
- Schär, C, M. Sprenger, D. Lüthi, Q. Jiang, R. B. Smith, and R. Benoit (2003): Structure and dynamics of an Alpine potential vorticity banner. *Q. J. R. Meteorol. Soc.*, **129**, 825–856.
- Smith, R. B. (1977): The steepening of hydrostatic mountain waves. *J. Atmos. Sci.*, **34**, 1634–1654.
- Smith, R. B. (1987): Aerial observations of the Yugoslavian bora. *J. Atmos. Sci.*, **44**, 269–297.
- Tudor, M., and Ivatek-Šahdan, S. (2002): MAP IOP 15 case study. *Cro. Met. Jour.* **37**, 1–14.
- Vučetić, V. (1984): On the time and space variations of the northern Adriatic bora. *Zbornik Meteorol. Hidrol. Radova*, **10**, 134–137.
- Vučetić, V. (2002): (Meteorological and Hydrological Service of Croatia, personal communication).

SAŽETAK

**Struktura mezoskalnog strujanja nad sjevernim Jadranom
tijekom MAP IOP 15 eksperimenta – slučaj jake bure**

*Zvezdana Bencetić Klaić, Danijel Belušić, Vanda Grubišić, Lada Gabela
i Ladislav Čoso*

Ispitali smo slučaj jake bure na sjevernom Jadranu, koji se dogodio 7. studenog 1999. tijekom MAP IOP 15 eksperimenta. Polja vjetra, potencijalne temperature, vertikalne komponente relativne vrtložnosti i turbulentne kinetičke energije u donjoj troposferi simulirana su nehidrostatskim mezoskalnim modelom (MEMO) s vrlo finom horizontalnom rezolucijom od 1 km. Simulacija je točno reproducirala nastup bure, a modelirana polja dobro su se podudarala s rutinski mjerenim vjetrom duž hrvatske obale te su pokazala visoku razinu konzistencije s MAP mjerenjima nad morem. Rezultati modela također su omogućili detaljan uvid u strukturu hidrauličkog toka te u termodinamičke uvjete tijekom bure. Rezultati simulacije potvrdili su postojanje topografski induciranih pruga vrtložnosti, koje nastaju u blizini obalnih planina, u turbulentnim područjima čiji položaj se podudara s tokom hidrauličkih svojstava. Svi ti procesi najintenzivniji su u području Senja.

Ključne riječi: bura, hidraulički tok, sjeverni Jadran

Corresponding author's address: Zvezdana Bencetić Klaić, Andrija Mohorovičić Geophysical Institute, Faculty of Science, University of Zagreb, Horvatovac bb, 10000 Zagreb, Croatia, e-mail: zklaic@rudjer.irb.hr.